LUND UNIVERSITY

A combined quantum and molecular mechanical study of the O-2 reductive cleavage in the catalytic cycle of multicopper oxidases

Rulisek, Lubomir; Solomon, E I; Ryde, Ulf

A QM/MM Study of the O$_2$ Reductive Cleavage in the Catalytic Cycle of Multicopper Oxidases

Lubomír Rulíšek,[§¶] Edward I. Solomon,[‡] and Ulf Ryde[†]*

Department of Theoretical Chemistry, Lund University, Chemical Center, P.O. Box 124, S–221 00 Lund, Sweden, E-mail: Ulf.Ryde@teokem.lu.se

Department of Molecular Modeling, Institute of Organic Chemistry and Biochemistry, Academy of Sciences of the Czech Republic, Flemingovo namesti 2, 166 10 Praha 6, Czech Republic

Department of Chemistry, Stanford University, Stanford, California 94305, U.S.A.

2004-12-21

[§] IOCB AS CR, Prague

[¶] most of the work was done during the postdoctoral stay at Lund University

[‡] Department of Chemistry, Stanford University

[†] Department of Chemistry, Lund University

* Corresponding author. Tel. (Fax): +46–46–2224502(4543).

Abstract: The four-electron reduction of dioxygen to water in multicopper oxidases takes place in a trinuclear copper cluster that is linked to a mononuclear blue copper site, where the substrates are oxidized. Recently, several intermediates in the catalytic cycle have been spectroscopically characterized and two possible structural models have been suggested for both the peroxy and native intermediates. In this study, these spectroscopic results are complemented by hybrid quantum and molecular mechanical (QM/MM) calculations, taking advantage of recently available crystal structures with a full complement of copper ions. Thereby, we obtain optimized molecular structures for all experimentally studied intermediates involved in the reductive cleavage of O_2 molecule and energy profiles for individual reaction steps. This allows identification of the experimentally observed intermediates and further insight into the reaction mechanism that is probably relevant for the whole class of multicopper oxidases. We suggest that the peroxy intermediate contains an O_2^{2-} ion, in which one oxygen atom bridges the type 2 copper ion and one of the type 3 copper ions, whereas the other one coordinates to the other type 3 copper ion. One-electron reduction of this intermediate triggers the cleavage of the O–O bond, which involves uptake of a proton. The product of this cleavage is the observed native intermediate, which we suggest to contain a O^{2-} ion coordinated to all three copper ions in the center of the cluster.

1. Introduction

The multicopper oxidases (MCO) are enzymes that couple four one-electron oxidations of a substrate with the four-electron reduction of molecular oxygen to water.[1,2]

$$O_2 + 4e^- + 4H^+ \xrightarrow{4Cu^{2+}} 2H_2O \tag{1}$$
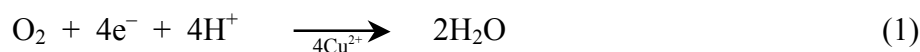
The most prominent and studied members of this family are laccase (Lc),[3,4] ascorbate oxidase (AO),[5] ceruloplasmin (Cp),[6] Fet3p (which along with Cp exhibits ferroxidase activity),[7] and CueO (part of the copper regulation system).[8]

All known MCOs contain at least four copper atoms, denoted according to the spectroscopic characteristics as type 1, type 2, and type 3 (T3). The type 1 copper (Cu1) is located at the substrate-binding site and is coordinated to one cysteine (Cys) and two histidine (His) residues. In most structures, it also binds to a fourth weak axial ligand, typically methionine. It shows a strong absorption around 600 nm, which arises from a S_{Cys}-to-copper charge-transfer excitation and gives rise to the intense blue color of the copper oxidases. The type 2 copper (Cu2) is located at one vertex of a trinuclear copper cluster. It is bound to two His residues and to a solvent molecule (cf. Figure 1). The two T3 copper ions have three His ligands each and are bridged by a solvent molecule in the oxidized state. They form an antiferromagnetically coupled pair and show a characteristic 330 nm absorption band arising from an $OH^- \rightarrow Cu^{II}$ charge-transfer transition. The four electrons necessary for the reduction of dioxygen are shuttled from Cu1 to the trinuclear cluster, where the reduction of O_2 takes place. The two sites are connected by a His–Cys–His peptide link (where Cys is a ligand of Cu1 and each of the two His residues is bound to one of the two T3 copper ions), which span a Cu–Cu distance of ~13 Å.

Eleven crystal structures of MCOs containing a full set of copper ions and with a resolution less than 2.5 Å [9,10,11,12,13,14,15] are available in the Protein Data Bank (December 2003).[16] In Table 1, the most important structural parameters of these are summarized. Because we are primarily interested in the oxygen reduction at the trinuclear copper cluster, the analysis will be restricted to this part of the structure. The general structure around this cluster is shown in Figure 1.

It can be seen that the Cu–Cu distances range between 3.5 and 5.1 Å, mainly depending on the oxidation state of the cluster (it is shorter in the oxidized than in the reduced structures). In most structures, the Cu–N$_{His}$ distances are 1.90–2.15 Å, with those of Cu2 being ~0.05 Å shorter than those of Cu3 and Cu3' (the two T3 copper ions). No correlation between these distances and oxidation state of copper ion can be discerned.

Almost all structures contain a ligand bridging the two T3 copper ions. The only exceptions are the reduced structure and two structures of AO with either azide or peroxide bound apically to one of the T3 copper ions.[12] In one case (laccase from *Melanocarpus*),[13] the bridging ligand is an O$_2$ molecule (the O–O distance is 1.20 Å) bound symmetrically between Cu3/3'. In all the other structures, a solvent molecule bridges the two T3 copper ions.

The reaction of fully reduced (i.e. by four electrons) MCOs has been studied by a number of spectroscopic techniques.[1,4,17,18,19,20,21,22] These have observed one intermediate in the reaction, called the *native intermediate* (NI). This is a four-electron reduced hydroxide product of the O–O bond cleavage, bound to a fully oxidized trinuclear cluster.[20] It has a total spin of 1/2 and shows electronic coupling over all three copper ions in the trinuclear cluster. The native intermediate decays to the resting oxidized state. However, this process is so slow that it is believed that it is the NI, and not the oxidized resting state, that is the catalytically relevant fully oxidized form of the enzyme.[20]
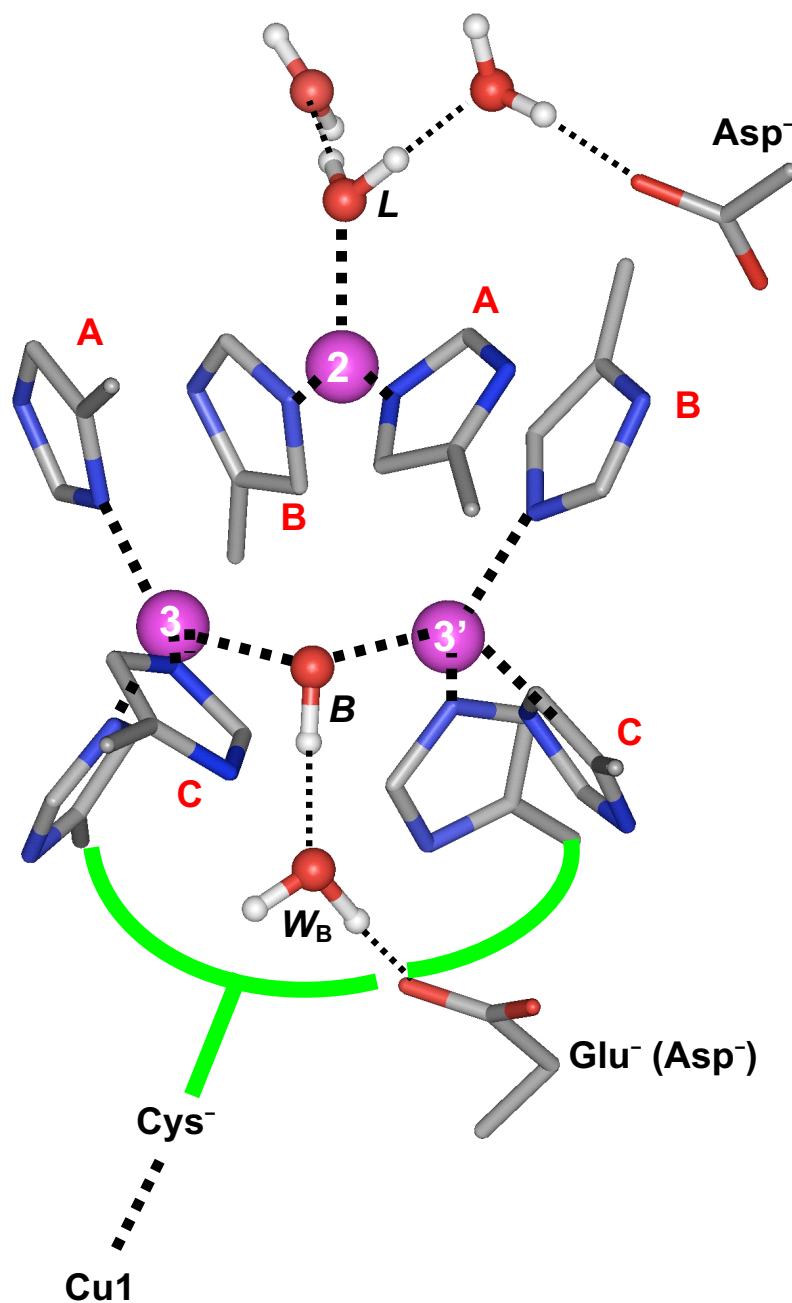
Figure 1. A schematic representation of the trinuclear copper cluster in the MCOs. All the His ligands are connected by a His–X–His motif and the corresponding pairs are marked by letters A–C. The fourth His–Cys–His pair is drawn schematically by the green line (Cys binds to Cu1). Coordination and hydrogen bonds are depicted by broken lines.

No other intermediates are observed in the reaction cycle of the native enzyme. However, if Cu1 is removed or replaced by a redox-inactive ion, a less reduced intermediate can be trapped.[17,18] It contains a two-electron reduced O_2 molecule, i.e., at the peroxide level, and is therefore called the *peroxy intermediate* (PI). It is formed at the same rate as the NI in the native enzyme and decays to a native-like intermediate at a slow rate, which depends on the protonation of a nearby residue. Therefore, it is believed to be a catalytically relevant intermediate also in the normal reaction cycle, indicating that the cycle consists of two two-electron reduction steps.

For both the native and peroxy intermediates, the spectroscopic studies have lead to two alternative structural interpretations, shown in Figure 2. The key feature of both structures for both intermediates is that the oxygen intermediate bridges between the T2 and T3 centers.[18,20] One suggestion for the PI has a O_2^{2-} ion in the center of the trinuclear cluster, with one oxygen atom coordinated to Cu2 and the other bridging between the two T3 copper ions (Fig. 2A, top). The other alternative has a HO_2^- ion at the periphery of the trinuclear cluster, with the unprotonated oxygen atom bridging between Cu2 and one of the two T3 copper ions (Fig. 2A, bottom). Recent studies of the Fet3p protein indicate that the former structure fits the experimental data best.
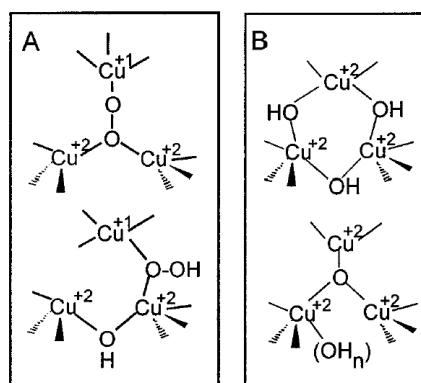
Figure 2. The structural models for PI (A) and NI (B) intermediates as suggested by spectroscopic measurements.[18,20]

Likewise, one possible model for the NI is a structure with three OH⁻ ions, each bridging two of the copper ions of the trinuclear cluster (Fig. 2B, top). The other alternative contains an O^{2-} ion

in the center of the trinuclear cluster (coordinating to all three copper ions) and with one or two solvent molecules coordinating to the T3 copper ions in a non-bridging manner (Fig. 2B, bottom). Finally, it should be noted that a crystal structure of the peroxide adduct of AO shows a third coordination mode of the peroxide, viz. terminal coordination to one T3 copper ion and with no bridging ligand between the two T3 Cu's (cf. Fig. 3g).[12]

Thus, despite all these achievements, some uncertainty still remains concerning the details of the reaction mechanism of O_2 reduction in MCOs. The goal of the present study is to see if a theoretical investigation may distinguish between the structural alternatives for the peroxy and native intermediates and yield a consistent picture of the reaction cycle. Quantum chemical investigations have been successfully used to study various properties of copper proteins.[23] In particular, several studies have been performed on hemocyanin,[24] tyrosinase,[25] and catechol oxidase,[26] which also contain a binuclear copper pair that binds and activates O_2. However, no quantum chemical investigation has evaluated the mechanism of O_2 reduction by the trinuclear cluster of MCOs. In this paper, we use combined quantum and molecular mechanics (QM/MM) methods to obtain structures and energetics of the peroxy and native intermediates, as well as the oxidized and reduced states of the MCOs.

2. Computational details

2.1. QM/MM procedure

All QM/MM calculations have been carried out with the COMQUM program.[27,28] In the current version, it uses Turbomole 5.6[29] for the QM part and AMBER 7[30] with the Cornell force field[31] for the MM part. In this approach, the protein and solvent are split into three subsystems: The QM region (system 1) contains the most interesting atoms and is relaxed by QM methods. System 2 consists of all the residues within 6 Å of any atom in system 1 and is relaxed by a full MM minimization in each step of the QM/MM geometry optimization. Finally, system 3 contains the

remaining part of the protein and surrounding solvent molecules and is kept fixed at the original (crystallographic) coordinates. In the quantum chemical calculations, the QM system is represented by a wave function, whereas all the other atoms are represented by an array of partial point charges, one for each atom, taken from Amber libraries. Thereby, the polarization of the quantum chemical system by the surroundings is included in a self-consistent manner. In the MM calculations, all atoms are represented by the Amber force field. When there is a bond between systems 1 and 2 (a junction) the hydrogen link atom approach is employed: The quantum region is truncated by hydrogen atoms, the positions of which are linearly related to the corresponding carbon atoms in the full system.[27,32] In order to eliminate the non-physical effect of placing point charges on atoms in MM region bonded to junction atoms (i.e., the closest neighbors of QM system), these are zeroed (a standard procedure in QM/MM methods).

The total energy is calculated as:

$$E_{tot} = E_{QM} + E_{MM123} - E_{MM1} \tag{1}$$

Here, E_{QM} is the QM energy of the quantum system truncated by the hydrogen atoms, excluding the self-energy of the surrounding point charges. E_{MM1} is the MM energy of the quantum system, still truncated by hydrogen atoms, but without any electrostatic interactions. Finally, E_{MM123} is the classical energy of all atoms in the system with normal atoms at the junctions and with the charges of the quantum system set to zero (to avoid double-counting of the electrostatic interactions). By using this approach, which is similar to the one used in the Oniom method,[33] errors caused by the truncation of the quantum system should cancel out. The calculated forces are the gradient of this energy, but owing to the differing junctions in the various calculations, they have to be corrected using the chain rule.

The geometry optimizations were carried out in two steps. First, systems 2 and 3 were frozen and only the quantum system was optimized (this structure will be referred to as *Protein_Fixed*).

Second, both systems 1 and 2 were allowed to relax. In the MM optimization of system 2, the charges on the quantum atoms were updated in each iteration of the QM/MM optimization. This optimization was performed with the looser convergence criterion of 10^{-4} a.u. for the change in energy and 10^{-2} a.u. for the maximum norm of Cartesian gradient (0.26 kJ/mol and 50 kJ/mol/Å). Then, system 2 was frozen again and the geometry optimization was continued with default convergence criteria (10^{-6} and 10^{-3} a.u.). The resulting structure will be denoted *Protein_Free* in the following. Such an approach was followed to get a feeling for the relaxation of the surrounding protein, but also to minimize artifacts caused by shortcomings of the MM force field.[34,35]

For complexes with more than one Cu^{II} ion, two electronic states are possible, depending on the coupling of the unpaired spins on the Cu^{II} ions. For these complexes, the two above calculations were performed for the ferromagnetically coupled state. One of the Cu^{II} spins was then reversed to obtain the antiferromagnetically coupled state and the quantum system was fully relaxed again with the default convergence criteria to obtain the final *Protein_Free* geometry. Such an approach is plausible, because the geometries of the anti- and ferromagnetically coupled states are very similar.

2.2. The protein

All QM/MM calculations were based on the 1.4-Å structure of CueO (PDB code 1KV7).[15a] This structure has been selected because it had the best resolution among the published MCO structures. In addition, it is a monomer and lacks glycosylated surface residues, which are common in the eukaryotic proteins. Hydrogen atoms were added to the crystal structure and this was solvated in a sphere of water molecules with a radius of 38 Å. The positions of the hydrogen atoms and solvent water molecules were then optimized by a 90-ps simulated annealing calculation with molecular dynamics followed by a conjugate gradient energy minimization of their positions. We assumed the normal protonation state at pH 7 for all amino acids, except for the copper-bound Cys residue, which was assumed to be deprotonated. For the His residues, the protonation status was decided form a detailed study of the hydrogen-bond network around the residue and the solvent accessibility. Thus, His-71, 111, 113, 393, 395, 446, and 448 were assumed to be protonated on the

$N^{\delta 1}$ atom, His-73, 390, and 452 on the $N^{\epsilon 2}$ atom, and the other eight His residues on both these atoms (the crystal was obtained at pH = 4.6). The space created by a disordered loop, missing in the CueO crystal structure (residues 380–402; more than 22 Å from the trinuclear copper cluster) was filled by water molecules.

It should be noted that recent results indicate that the Cu3/3' bridging ligand, which is modeled as an OH⁻ ion in the crystal structure, may be a chlorine anion instead.[15b] However, this should not affect our structures, because we relax the surrounding protein.

2.3. Quantum chemical calculations

All quantum chemical calculations have been performed with density functional theory. Geometry optimizations were carried out at the Becke–Perdew86 (BP86) level.[36] These calculations were sped up by expanding the Coulomb interactions in an auxiliary basis set, the resolution-of-identity (RI) approximation.[37,38] They employed the 6–31G* basis set on all atoms except Cu, for which we used the DZP basis set of Schäfer et al., enhanced with p, d, and f-type functions with coefficients of 0.174, 0.132, and 0.39, respectively.[39,40] Accurate single-point energies were then calculated on these geometries with the B3LYP method[41] as implemented in Turbomole.[42] These calculations employed the 6–311+G(2d,2p) basis set[43] and the basis set on Cu was enhanced with s, p, and f functions with coefficients of 0.0155, 0.046199, and 3.55, respectively. Both ferromagnetically coupled states (S = 3/2 for Ox and NI; S = 1 for PI) and antiferromagnetically coupled states (S = 1/2 or 0, respectively) have been calculated for all the species containing at least two Cu^{II} ions.[44] The broken-symmetry approach was employed to obtain the low-spin states.[45]

In order to study the detailed effect of the protein surrounding, we have also carried out geometry optimizations of some complexes in a dielectric continuum, using the COSMO[46,47] method. These calculations were performed at the BP86 level of theory, using default values for all parameters (implying a water-like probe molecule) and a dielectric constant (ε_r) of 80. For the generation of the cavity, a set of atomic radii has to be defined. We used the optimized COSMO radii[48] in Turbomole and 2.0 Å for Cu.

2.4. Model systems and nomenclature

The QM system in the QM/MM calculations consisted of the three Cu ions in the trinuclear cluster, eight imidazole (Im) molecules (models of the histidine ligands, truncated at the C^β atom), the solvent molecule bridging Cu3 and Cu3' (B) and a water molecule hydrogen-bound to it (W_B, cf. Figure 1), the solvent molecule coordinated to Cu2 (L), and possibly additional O_2-derived ligands (e.g., O_2, HO_2^-, $2 \times O^{2-}$). These contained a total of 80–87 atoms. System 2 consisted of 71 amino acids and 13 H_2O molecules, whereas System 3 is the rest of protein and water molecules (in total 469 residues and 4339 water molecules). All the details of the structure setup, including the position of all hydrogen atoms after equilibration, partial charges in MM region, and residue names can be found from a sample PDB file in the supplementary material.

The situation is complicated by the fact that both the O_2-derived molecule and copper-bound solvent molecules may have varying protonation states: O_2, HO_2, and H_2O_2 (with a varying net charge depending on the oxidation state) for the former, and H_2O, OH^-, or O^{2-} for L and B, and the O_2 ligand after O–O bond cleavage. Moreover, the ligands may also be missing. We assume that W_B is always present and neutral (H_2O), unless explicitly stated. In the following we will define the various states by listing explicitly the nature of the ligand and the protonation state for each of the ligands in the order {L,B,O_2-derivative}. A missing L or B ligand is marked by a dash, e.g. {–,–,HO_2^-}.

Finally, the ligands, especially the O_2 derivative, may bind in many different positions in the cluster. A single O^{2-} ion may bind in the center of the cluster, coordinated to all three copper ions. Such a coordination will be denoted C (O^{2-}:C; cf. Fig. 3a). An O_2 molecule (possibly protonated) may also bind in the center of the cluster, and the O–O bond may then be either parallel ($C_{\parallel}$; cf. Fig. 3b) or perpendicular ($C_{\perp}$; cf. Fig. 3c) to the Cu3–Cu3' bond. It may also bind on the side, with one of the oxygen atoms bridging two copper ions. This conformation will be denoted S_{23}, $S_{23'}$, or $S_{33'}$, depending on which two copper ions are bridged (Figs. 3d-f). Finally, the O_2 derivative (as well as

B) may bind to only one T3 copper ion, which will be denoted as A_3 or $A_{3'}$ (apical binding; cf. Figs. 3g and h). If no binding mode is given, it is assumed that *L* binds in the A_2 position (Figure 3i) and *B* binds in the $S_{33'}$ mode. With this nomenclature, the two suggested states for both the peroxy and native intermediates, given in the introduction (Figure 2), are $\{L,-,O_2{}^{2-}:C_\perp\}$ or $\{L,B,HO_2{}^-:S_{23/3'}\}$ and $\{L,OH^-,OH^-:S_{23},OH^-:S_{23'}\}$ or $\{L,(OH^-:A_{3/3'})_n,O:C\}$.
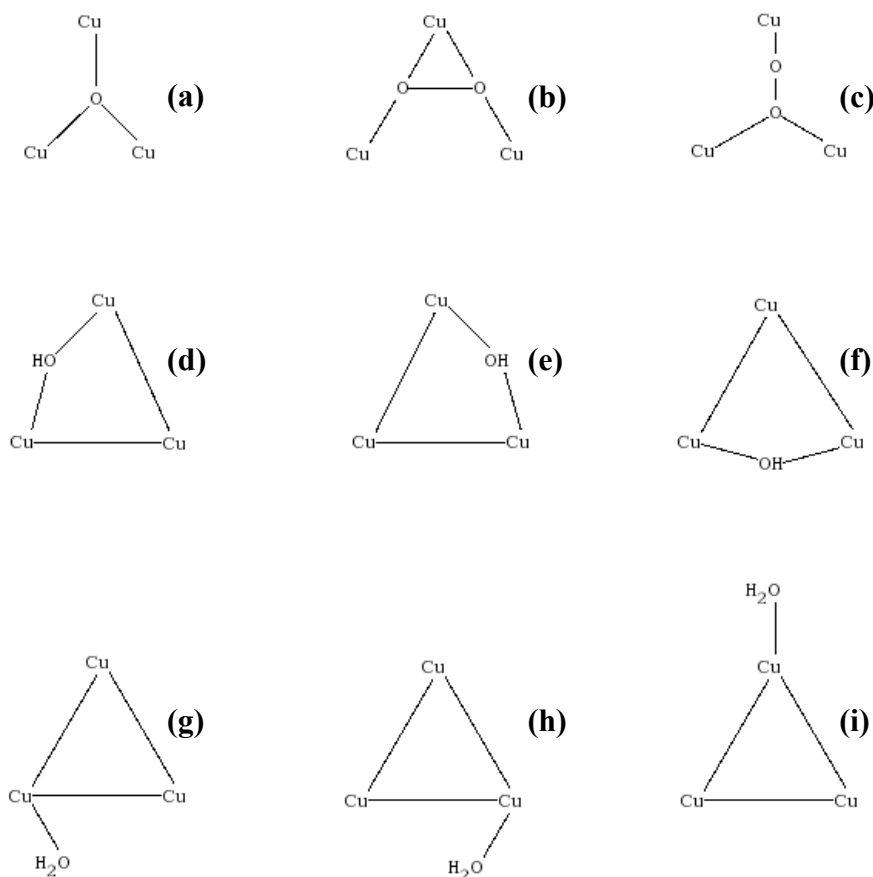
Figure 3. A schematic explanation of the nomenclature used in this study. In all figures the T2 copper is on the top, Cu3 is on the left side, and Cu3' is on the right side. (a) O:C, (b) O_2:C$\|$, (c) O_2:C$_\perp$, (d) OH:S_{23}, (e) OH:$S_{23'}$, (f) OH:$S_{33'}$, (g) H_2O:A_3, (h) H_2O: $A_{3'}$, (i) H_2O:A_2.

Consequently, there are quite few possibilities for Ox and Red structures, viz. the combination of the protonation states of *L* and *B*. There are additional possibilities for the orientation and protonation of the O_2-derived ligand in the peroxy and native intermediates. Initially, most of the

reasonable combinations of possible protonation states and coordination modes were tested in vacuum (including some tests calculations with deprotonated imidazole ligands). Based on these results, the most interesting states were selected for QM/MM studies. For the QM/MM results, Cu3 is the copper ion ligated to His-143, 448, and 499, whereas Cu3' is bound to His-103, 141, and 501 (called Cu2 and Cu3 in the PDB file, respectively).

3. Results and Discussion

3.1. Structures and energies

This investigation of the MCOs is based on a great number of vacuum and continuum-solvent QM calculations followed by and integrated with ~150 QM/MM calculations of the trinuclear copper cluster in various oxidation states and with different B, L, and O_2-derived ligands. In most cases, the three types of calculations gave similar results. Therefore, we will mostly describe only the QM/MM structures. However, when interesting, we will also discuss similarities and differences with the vacuum and continuum solvent calculations.

The most conspicuous difference between the vacuum and QM/MM calculations is that many complexes (especially the oxidized and reduced states) dissociated into fragments in vacuum (typically a bridged binuclear copper center and an isolated mononuclear copper center). For the oxidized complexes, this is an effect of the high net charge of these clusters. In the protein, this charge is compensated by the two conserved carboxylate groups shown in Figure 1, and by the dielectric screening of the surrounding protein bulk. In most proteins, there are additional negatively charged groups close to the copper site. For example, there are seven carboxylate groups, one arginine, one lysine within 6 Å of the copper cluster in CueO, resulting in the total charge of –5 for this region (system 2 in our calculations). This is confirmed by the calculations in a dielectric continuum ($\varepsilon_r = 80$), which gave stable structures for most of the complexes studied.

For the reduced models, the dissociation is most likely caused by the weak Cu^I–ligand interaction: In vacuum, it is more favorable for the imidazole groups to form hydrogen bonds to the other ligands, especially as these are strengthened by the polarizing effect of the metal, than to bind directly to the metal. In the protein, these hydrogen-bond sites are occupied by interactions with the surrounding protein. Also for the reduced structures, optimizations in a dielectric continuum gave stable structures for all complexes. For most of the intermediates, the structures did not dissociate in vacuum.

The results of the QM/MM calculations (geometric data, electronic structure, spin-splitting, and relative energies) are collected in Tables 2–5. Structural data are presented only for the antiferromanetically coupled (if applicable) *Protein_Free* calculations. The effect of the antiferromagnetic coupling on the active site geometry is fairly small, typically leading to changes of ~0.03 Å for the Cu–Cu distances (maximum change 0.11 Å), and ~0.01 Å for the Cu–*L* distance. In the following, we will discuss the results for each oxidation state in separate sections.

3.1.1. Oxidized state. Ten QM/MM structures were obtained for the oxidized (Ox) state, differing in the protonation and binding positions of the *L* (H$_2$O or OH$^-$) and *B* (H$_2$O, OH$^-$, or O^{2-}) ligands. Most of these are described in Table 2. We tested four structures with an OH$^-$ ion bridging Cu2 and Cu3/3' (rather than Cu3 and Cu3'), viz. {OH$^-$,–,OH$^-$:S$_{23/3'}$} and {–,OH$^-$,OH$^-$:S$_{23/3'}$}. However, all these structures were 139–202 kJ/mol less stable than the most stable other structures (if not otherwise stated, energies cited in the text are total energies with and without the MM energy as a range, i.e. ΔE_{tot} and ΔE_{totMM} using the nomenclature in Table 5). Moreover, we also tried in vacuum many structures with deprotonated Im ligands. However, all these structures were at least 40 kJ/mol less stable than other protonation states (80 kJ/mol with two deprotonated Im molecules). This is in accord with the lack of imidazolate-to-copper charge-transfer transitions in the spectrum of the oxidized resting state of the MCOs.[49]

The calculation with $B = H_2O$, i.e. $\{OH^-,H_2O\}$, gave a long Cu3–Cu3' distance (5.4 Å) and an unsymmetrical binding of the water molecule. Such features are not consistent with the spectroscopy (the T3 copper ions are antiferromagnetically coupled) nor observed in crystal structures of oxidized MCOs, showing that this is not the correct protonation state of the B ligand. This is further corroborated by the fact that this structure is 40–52 kJ/mol less stable than the $\{H_2O,OH^-\}$ structure, in agreement with the expectation that it would be more favorable to deprotonate a ligand bridging two copper ions than a terminal ligand.

The two calculations with $B = O^{2-}$ (as well as all vacuum and continuum solvent calculations with $B = O^{2-}$) resulted in structures where O^{2-} was located in the center of the trinuclear cluster (O^{2-} :C). This is somewhat unexpected because we included in the quantum system the water molecule (W_B) that bridges the B ligand and the negatively charged Asp/Glu group that is bordering QM region from the MM side, further polarizing W_B (cf. Figure 1). Thus, it can donate a hydrogen bond to the carboxylate group and it may donate and accept a hydrogen bond to B, but there is no further hydrogen-bond partner in its neighborhood. Therefore, it would be quite favorable for it to donate a hydrogen bond to O^{2-} in an $S_{33'}$ position. Moreover, the QM/MM calculation would allow for a proton transfer from this water molecule to the O^{2-} group, if this would lead to an energetically improved structure. This is not observed, however.

Such an (O^{2-}:C) coordination is not consistent with the spectroscopy on resting state and has not been observed in any of the available crystal structures of oxidized MCOs having Cu–Cu distances of 3.8–3.9 Å, appreciably longer than in these calculated structures (3.1–3.5 Å). Therefore, it seems unlikely that the bridging ligand is O^{2-} in the oxidized crystal structures. However, the $\{H_2O,O^{2-}\}$ state is actually 66 kJ/mol *more* stable than the tautomeric $\{OH^-,OH^-\}$ state (in vacuum or a dielectric continuum the difference is 22 and 51 kJ/mol, respectively). We have at present no good explanation why the $\{L,O^{2-}\}$ structures are not observed in crystals, although they are energetically more stable (but we will see below that such a structure may be present in the native intermediate).

We have tested if the W_B water molecule may protonate the O^{2-} ion, by optimizing the {OH^-,OH^-} state with W_B deprotonated. However, during the geometry optimization, a proton migrated from the bridging OH^- to W_B, giving a structure that was essentially identical to the {OH^-,O^{2-}} state.

The best agreement with the crystal structures is achieved for the {OH^-,OH^-} and {H_2O,OH^-} states, with Cu–Cu distances of 3.8–4.1 Å and 3.8–4.2 Å, respectively. Thus, our results indicate one of these two protonation states is observed experimentally. The Cu–Cu distances for the {OH^-,OH^-} state is slightly closer to those in the crystal structures (by ~0.1 Å in Cu2/3'). On the other hand, the Cu2–L distance in the {H_2O,OH^-} state (2.12 Å) is in better agreement with that observed in the three oxidized structures (2.0–2.4 Å) than the {OH^-,OH^-} state (1.87 Å). Energetically, the two structures are not directly comparable, but if the structures are optimized in a dielectric continuum with the Cu–Cu distances constrained to the crystal values, the {OH^-,OH^-} state is less destabilized (by 2 kJ/mol compared to the fully optimized structure) than the {H_2O,OH^-} state (22 kJ/mol). Moreover, experimental data indicate that L is deprotonated to OH^- throughout the physiological pH range.[50] Therefore, we conclude that {OH^-,OH^-} is the protonation state observed in the oxidized crystal structures.

The calculated spin densities for the ferro- and antiferromagnetically coupled electronic states are listed in Table 4. They can be used to assign the formal oxidation states of copper ions and to study the spin coupling between the copper ions. It can be seen that the two spin-coupling schemes give quite similar results (disregarding the sign of the spin), although the antiferromagnetically coupled states in general have somewhat lower spin densities, especially on O_B. The spin densities on copper ions are 0.4–0.8 e with the remaining spin delocalized on the ligands. Water molecules have negligible spin, whereas OH^- and O^{2-} have a spin of 0.1–0.5 e, except when bridging two antiferromagnetically coupled copper ions. The spin is in general higher on the L ligand than on the B ligand. In most of the structures, Cu3 and Cu3' are antiferromagnetically coupled, but in {H_2O,OH^-} and {OH^-,O^{2-}}, it is instead Cu2 that has spin of the opposite sign. This may seem

16

strange, but we have checked thoroughly that there are no other antiferromagnetically coupled states that are lower in energy. Still, the preferred {OH⁻,OH⁻} model has the expected antiferromagnetic coupling between the two T3 copper ions.[2]

An important quantity is the energy difference between the ferro- and antiferromagnetically coupled states. Experimentally, it is quantified by the value of the J coupling constant. The calculated values of the energy difference between the ferro- and antiferromagnetically coupled states (ΔE_{spin}) are listed in Table 4. They are quite small, less than 20 kJ/mol. For the most interesting state, {OH⁻,OH⁻}, the antiferromagnetically coupled state is 11 kJ/mol more stable than the ferromagnetically coupled state, in agreement with the observed doublet ground state.[2] The same applies for all the protonation states, except {OH⁻,O²⁻}.

3.1.2. Reduced state. For the reduced state (Red), eight structures were optimized with various protonation states of the L and B ligands (H_2O, OH⁻, or −). The results are quite similar to those of the oxidized state: With $B = H_2O$, a long Cu3–Cu3' distance is obtained (5.0–5.2 Å) and the binding of H_2O is asymmetric (one of the Cu3–O distances is 2.1–2.3, the other 2.7–3.5 Å). Moreover, the {H_2O,OH⁻} state is 59–104 kJ/mol more stable than the {OH⁻,H_2O} state (30 and 38 kJ/mol in vacuum and in a dielectric continuum, respectively), again confirming that a bridging water is more easily deprotonated than a terminal one.

With $B = $ OH⁻, the Cu3–Cu3' distance is much shorter, 4.0–4.3 Å. The {H_2O,OH⁻} state gives a strange structure with OH⁻ in the center of the trinuclear cluster and with the two Cu2–Cu3 distances of 2.8–2.9 Å. A similar structure is also obtained in vacuum and in a dielectric continuum.

The Cu3–Cu3' distances in the complexes with no B ligand are similar to those with $B = H_2O$, ~5.2 Å. These are the structures that are most similar to the crystal structure of reduced AO (which also lacks a B ligand).[12] All Cu–Cu distances of the {H_2O,−} structure are slightly closer to the crystal structure than those of the {OH,−} structure, but the difference is less than 0.1 Å. However, the Cu2–O_L distance in the {OH,−} structure (1.94 Å) is closer to that in the crystal (2.18 Å) than

that in the $\{H_2O,-\}$ structure (2.62 Å). It is a general problem in our calculations that the $L = H_2O$ ligand tends to form too long a bond to Cu2 in most structures, perhaps indicating that the quantum system should have been extended to include the water molecules and the Asp residue connected to the L ligand (cf. Figure 1) to obtain more accurate geometries of this ligand. Therefore, we suggest $\{H_2O,-\}$ as the best model of the reduced state of the MCOs.

Finally, it is notable that the Cu–N$_{His}$ distances are not very different from those of the oxidized complexes (there is a tendency to shorten at least one of the Cu–N$_{His}$ distances of Cu3, but the difference is less than 0.1 Å). Thus, these distances show only a minor variation between the various oxidation states of the trinuclear copper cluster and will not be further discussed.

3.1.3. Peroxy intermediate. The PI is one of the two key intermediates in the catalytic cycle of the MCOs. It is formally a $Cu^I Cu^{II}_2 O_2^{2-}$ complex with Cu1 in the reduced state. Fifteen distinct models of this intermediate have been obtained from QM/MM optimization of molecular geometry and are described in Tables 3 (geometries), 4 (spin densities), and 5 (relative energies). They differ in the protonation state of the O_2 (O_2^{2-}, HO_2^-, or H_2O_2), B, and L (H_2O, OH^-, or none) ligands, as well as in the binding mode of the O_2-derived ligand.

As was discussed in the introduction, three binding modes of the peroxide ligand have been suggested: in the center of the trinuclear cluster ($C_\perp$), on one of the sides of the cluster ($S_{23/3'}$), or as a terminal ligand of one of the T3 copper ions ($A_{3/3'}$), cf. Figures 2A and 3e. We have tried hard to obtain all three structures, both in the protein, in vacuum, and in a continuum solvent. Interestingly, independently on the starting structures, only two coordinating modes were observed in the optimized structures. One was the $S_{23/3'}$ mode, where one of the oxygen atoms bridges Cu2 and Cu3/3', whereas the other (the protonated one for HO_2^-) points out of the trinuclear cluster. This structure is depicted in Figure 4.
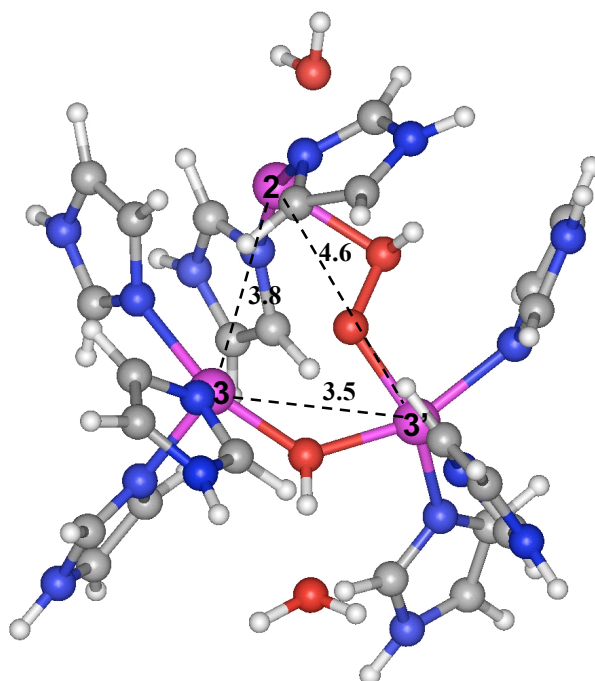
Figure 4. The $\{H_2O,OH^-,HO_2^-:S_{23'}\}$ structure, illustrating the S_{23} binding mode of the PI. Note the distorted coordination of some of the imidazole ligands.

In the other mode, the peroxide was bound in the center of the trinuclear cluster, but not in the $C_\parallel$ or $C_\perp$ conformations, but rather in an intermediate, diagonal, mode with one oxygen atom coordinated to Cu3'and the other atom bridging Cu2 and Cu3. We will call this binding mode $C_{3'}$; it is illustrated in Figure 5. No structure with the $A_{3/3'}$ coordination mode was obtained, even if optimizations (both in vacuum and in the protein and with various protonation states of the B and L ligands) were started in this coordination mode.
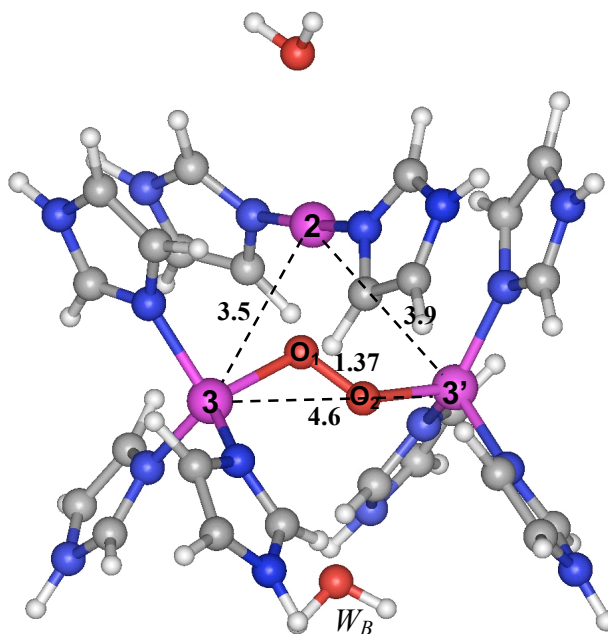
Figure 5: The {H_2O,–,O_2:$C_{3'}$} structure, illustrating the $C_{3'}$ binding mode.

Most of the structures ended up in the $C_{3'}$ binding mode and showed only small changes in the structure, compared to the crystal structure. With O_2 binding in this mode, the three Cu–Cu distances were 3.4–3.6, 3.8–3.9, and 4.4–4.6 Å, independent of the *B* and *L* ligands and if the optimization was performed in vacuum, in a dielectric continuum, or in the protein. Quite surprisingly, the same distances were also obtained for the C_3 binding mode (where one of the oxygen atoms binds to Cu3 rather than Cu3'), for which it could have been expected that Cu2–Cu3 and Cu2–Cu3' distances were interchanged. This shows that the protein favors shorter Cu2–Cu3 (rather then Cu2–Cu3') distances. This is also observed in most of the other complexes (in the crystal structure the difference is 0.44 Å). The shorter of the Cu–Cu distances (3.45–3.57 Å) is in reasonable agreement with the observation of a Cu–Cu interaction of 3.4 Å in EXAFS experiments of the PI.[17] The two modes have essentially the same energy, with the C_3 mode being 4–9 kJ/mol more stable than the $C_{3'}$ mode (Table 5).

Only a few calculations converged to the $S_{23/3'}$ coordination mode. It was only obtained in the presence of bridging *B* ligand (if it was removed, the structures reorganized to the C_3 mode). Moreover, all these structures showed some awkward interactions (short distances between Cu and

20

carbon atoms in Im or with copper ions significantly displaced out of the plane of their Im ligands; cf. Figure 4). This indicates that the $S_{23/3'}$ structures are disfavored in the protein – there is simply not enough space for the O_2-derived ligand on the side of this sterically crowded cluster. This is also confirmed by the fact that all $S_{23/3'}$ structures in vacuum or a dielectric continuum lost one or more Im ligands. Moreover, in two of the QM/MM structures, the shortest Cu–Cu distance is only 2.8 or 3.0 Å, which is much shorter than observed by EXAFS (3.4 Å). However, in the $\{H_2O,OH^-,O_2^{2-}/HO_2^-:S_{23'}\}$ structures, the shortest interaction is 3.42-3.53 Å, which is similar to that in the C_3 structures. The latter structures are by 36–50 kJ/mol the most stable among the $S_{23/3'}$ structures (except for the O_2 complex with the MM term, -17 kJ/mol).

Unfortunately, it is hard to get a direct estimate of the relative energy of the $S_{23/3'}$ and $C_{3/3'}$ binding modes in the protein, because the former structures have a bridging B ligand, whereas the latter do not. The $\{H_2O,H_2O/OH^-:A_3,O_2^{2-}:C_{3'}\}$ structures were set up for this purpose, because their energies are comparable to the $S_{23/3'}$ structures (which must have a B bridging ligand). Even if the $H_2O/OH^-:A_3$ ligands are unnatural for the $C_{3'}$ mode, the $\{H_2O,OH^-:A_3,O_2^{2-}:C_{3'}\}$ structure turned out to be 44–97 kJ/mol more stable than the $\{H_2O,OH^-,O_2^{2-}:S_{23}\}$, and 65–122 kJ/mol more stable than the $\{OH^-,OH^-,HO_2^-:C_\perp\}$ structure (which was actually started in the $S_{23'}$ mode). Likewise, the $\{H_2O,H_2O:A_3,O_2^{2-}:C_{3'}\}$ structure is 24–130 kJ/mol more stable than the $\{H_2O,OH^-,HO_2^-:S_{23/3'}\}$ structures, despite the fact that the $H_2O:A_3$ molecule is loosely bound and makes the interactions with the surrounding enzyme less favorable. These comparisons clearly indicate that the $C_{3/3'}$ state is more favorable, by at least 24 kJ/mol (even if an unfavorable B ligand has been added to the $C_{3/3'}$ state). In vacuum and a dielectric continuum, the $C_{3'}$ mode is still more stable than the $S_{23'}$ coordination modes, but the difference is only 5–10 kJ/mol, showing that the main discrimination comes from the surrounding protein (however, it should be noted that the vacuum energies were obtained for complexes with one or more dissociated Im ligands, which would favor the crowded S_{23} mode).

An even larger discrimination is obtained if we delete the B ligand in the $S_{23'}$ state (which would disfavor this state in the same way as the OH^-:A_3 ligand disfavors the C_3 state): From Table 5, it can be seen that the $\{H_2O,-,O_2^{2-}:C_{3'}\}$ structure is 40–65 kJ/mol more stable than the $\{OH^-,-,O_2H^-:S_{23'}\}$ and $\{H_2O,-,O_2^{2-}:S_{23'}\}$ states in vacuum and a dielectric continuum. Likewise, the $\{OH^-,-,O_2^{2-}:C_{3'}\}$ state is 38–53 kJ/mol more stable than the $\{OH^-,-,O_2^{2-}:S_{23'}\}$ state (as was mentioned above, such an $S_{23/3'}$ starting structure without any B ligand reorganized to the $C_{3/3'}$ state in the protein). Thus, we can safely conclude that the $C_{3'}$ coordination mode of the O_2–derived ligand is more stable than the $S_{23'}$ mode, especially in the protein environment.

The protonation state of the peroxide ligand is unclear. It binds as a neutral O_2 molecule, which is reduced by internal electron transfer, and should then be successively protonated to finally form two water molecules. If two protons are added (giving H_2O_2), it automatically dissociates into two OH moieties during the geometry optimizations (no stable structure with H_2O_2 bound to the trinuclear copper cluster is found in the protein, vacuum, or solvent continuum calculations). This is associated with a considerable weakening of one of the Cu3–Im bonds (2.7 Å), because one of the OH^- ions binds to the Cu3 ion in a square-planar fashion (and forms a hydrogen bond to another OH^- molecule), with the weakly bound Im residue as the axial ligand. The spin density (Table 4) shows that two of the copper ions (Cu2 and Cu3') are oxidized and antiferromagnetically coupled (spin density of 0.6–0.7 e), whereas the third (Cu3) has no spin. The spin on the OH^- ligands is quite small (0.03–0.18 e). Together, these clearly indicate that the Cu3 ion has been oxidized to the Cu^{III} state and H_2O_2 has been reduced to two OH^- ions. However, even if this shows the facile breaking of the O–O bond and that it can be triggered by protonation, it is unlikely that this represents an intermediate in the catalytic cycle of MCOs.

For the HO_2^- state in the $C_{3/3'}$ mode, the hydrogen atom can point in two directions, either towards the Cu2 ion (denoted H_up in the tables) or towards the W_B molecule. The latter conformation is more stable by 22–27 kJ/mol and gives structures similar to those of the O_2^{2-} complexes, whereas the H_up structure gives longer Cu2–Cu3/3' bonds of 4.1–4.3 Å. The spin

densities in Table 4 show that HO_2^- has low spin density of 0.1–0.3 e, in accordance with its interpretation as a hydroperoxide ion. This is also corroborated by a long O–O bond, 1.44–1.46 Å. The ferro- and antiferromagnetically coupled states are close in energy, with the former state more stable by 0–5 kJ/mol. In the latter states, any pair of copper ions may be coupled, depending on the L ligand.

For the O_2^{2-}:$C_{3'}$ complexes, our calculations indicate that the ferromagnetically coupled states are most stable by 6–20 kJ/mol. This is not in agreement with experimental results, which show that the peroxy intermediate is diamagnetic (i.e., Cu3/3' pair is antiferromagnetically coupled).[17] However, all calculated ΔE_{spin} are less than 20 kJ/mol and thus within the error bar of our method. Moreover, it is well known that DFT methods overestimate the delocalization,[51] which would be expected especially for these mixed-valence $Cu^I Cu_2^{II}$ structures. This is confirmed by preliminary calculations with a more accurate method, second-order perturbation theory on a complete active space self-consistent field wave function (CASPT2),[52] which give an antiferromagnetically coupled ground state by 3 kJ/mol for O_2^{2-}:$C_{3'}$ state.[53] Therefore, ΔE_{spin} cannot be used to discard the C_3 coordination mode. On the contrary, all the other results strongly favor the C_3 mode, indicating that the S_{23} mode is hard to obtain, sterically crowded, and energetically disfavored by at least 24 kJ/mol, even with an unfavorable B ligand for the $C_{3'}$ state.

If we conclude that it is the C_3 binding mode that is observed experimentally, the next question is whether O_2 is protonated or not. Experimentally, it is clear that no external proton is involved in the formation of the PI.[18] This indicates that either O_2 is not protonated or that it takes its proton from one of the copper ligands. We have seen that the Red state is most likely {H_2O,–}. Consequently, PI must be either {H_2O,–,O_2^{2-}} or {OH^-,–,HO_2^-} (once deprotonation of W_B water has been ruled out). However, the results in Table 5 clearly show the former state is 58–98 kJ/mol more stable (46–72 kJ/mol in vacuum or a dielectric continuum). Therefore, we suggest that the experimentally observed peroxy intermediate is {H_2O,–,O_2^{2-}:C_3}.

From Table 4, it can be seen that this complex in the experimentally observed antiferromagnetically coupled state has essentially no spin on Cu2 and L, whereas the two Cu3 ions are antiferromagnetically coupled with 0.2–0.4 spins each and with some spin also on the O_2^{2-} ligand (0.2 e). This is in reasonable accordance with the experimental X-ray K-edge absorption results, which show that two copper ions are oxidized,[17] and therefore confirm the interpretation of this complex as a peroxide-level intermediate.

3.1.4 Peroxide adduct to the oxidized structure. This state (PA) is obtained by adding H_2O_2 to the oxidized state of MCOs, giving a state (formally $Cu^{II}_3O_2^{2-}$) that is one step more oxidized than the peroxy intermediate.[54] PA is not relevant for the catalytic cycle of MCOs, but it has been included in our study from two reasons: First, it has been spectroscopically characterized and the same two structural interpretations as for the peroxy intermediate have been proposed ($C_{3/3'}$ and $S_{23/3'}$, cf. Figure 2). Second, most of its spectroscopic characteristics are very similar to those of the peroxy intermediate. Therefore, we can employ data of PA to elucidate the structure of the peroxy intermediate.

Five structures of PA have been studied: $\{OH^-,-,O_2^{2-}:C_{3/3'}\}$, $\{OH^-,H_2O:A_3,O_2^{2-}:C_3\}$, and $\{OH^-,OH^-,HO_2^-:S_{23/3'}\}$, covering the suggested structural alternatives. One of the structures - $\{OH^-,OH^-,HO_2^-:S_{23}\}$ - ended up in the strange $\{OH^-,OH^-,HO_2^-:C_\perp\}$ H_up conformation, with a dissociated Im ligand on Cu3' (but this once again illustrates that it is hard to obtain the $S_{23/3'}$ binding mode, owing to the steric crowding). The geometries of the optimized structures are included in Table 3. EXAFS measurements have identified a Cu–Cu distance of 3.4 Å for PA.[54] It can be seen that the only structure that gives a Cu–Cu distance close to this is the $\{OH^-,-,O_2^{2-}:C_{3'}\}$ structure (3.52 Å; the $\{OH^-,OH^-,HO_2^-:S_{23'}\}$ structure gave two Cu–Cu distances of 3.72 Å). Energetically, it is 9–12 kJ/mol more stable than the $\{OH^-,-,O_2^{2-}:C_3\}$ isomer (with a Cu–Cu distance of 3.66 Å). The plausibility of this binding mode is further corroborated by the fact that the $\{OH^-,H_2O:A_3,O_2^{2-}:C_3\}$ complex is 35–53 and 149-179 kJ/mol more stable than the $\{OH^-,OH^-,HO_2^-$

:$C_\perp$} and {OH^-,OH^-,HO_2^-:$S_{23'}$} structures, respectively, despite that the former has an extra B ligand.

As for the PI, the {OH^-,OH^-,HO_2^-:$S_{23'}$} structure is antiferromagnetically coupled, whereas for the other four complexes, the ferromagnetically coupled spin state is 2–7 kJ/mol more stable than the antiferromagnetically coupled state, which is in variance with the observed doublet (S=1/2) ground state.[54] However, as discussed above, these energies are within the error limit of the method. ΔE_{spin} is smaller than for peroxy intermediate, indicating the above discussed shortcoming of DFT methods is smaller in Cu_3^{II} redox state, as expected. Again, the more accurate CASPT2 method gives an antiferromagnetically coupled ground state (by 2 kJ/mol) for the {OH^-,–,O_2^{2-}:$C_{3'}$} state.[53] The spin densities on the copper ions predict that Cu2 is antiferromagnetically coupled with one of the T3 copper ions in all except the {OH^-,OH^-,HO_2^-:$C_\perp$} structure.

In conclusion, we have obtained a number of results indicating that it is the (H)O2:$C_{3/3'}$ mode that is observed experimentally for the PI and PA state. First, the $C_{3'}$ binding mode is always energetically more favorable than the $S_{23'}$ mode, even if this state is destabilized by the addition of an artificial B ligand. Second, the shortest Cu–Cu distance of 3.5–3.6 Å is close to the experimental value of 3.4 Å for the C_3 mode, but not for the $S_{23/3'}$ mode. Third, the $C_{3/3'}$ PI and PA states have almost identical structure and electronic states, in agreement with the spectroscopic observations.[54] Fourth, most geometry optimizations (also those started in the A_3 and $C_\perp$ modes) converged to C_3 structure. Fifth, all $S_{23/3'}$ structures are awkward and seemingly strained. Finally it is notable that in no case an $A_{3/3'}$ type coordination is obtained, in contrast to what is observed in the crystal structure of AO.[12]

3.1.5 Native intermediate. In the native intermediate, an electron has been added to the PI (i.e. to formally yield $Cu_2^I Cu^{II} O_2^{2-}$), which leads to cleavage of the O–O bond, with uptake of protons (i.e. formally $Cu_3^{II}(OH^-)_2$). The latter structures are at the same oxidation level as the oxidized state. We will denote these two types of native intermediate structures NI' and NI (before and after the

cleavage of the O–O bond). Ten structures of each type were studied, varying in the protonation state of the L and B ligands (H_2O, OH^-, O^{2-}, or vacant), the state of the O_2-derived ligand (O_2^{2-}, HO_2^-, H_2O_2, 2 OH^-, $OH^- + O^{2-}$, or 2 O^{2-}), and the binding mode of the latter. In all the calculations, we assumed that Cu1 is in the oxidized state.

The results for NI' structures with the O_2^{2-} and HO_2^- are similar to those of PI and PA: Stable and unstrained structures were obtained for the $C_{3'}$ binding mode for both ligands and the Cu–Cu distances were similar to those of the PI and PA structures, 3.3–3.5, 3.7–4.2, and 4.6–4.9 Å (Table 3). In analogy with the peroxy intermediate, it was more favorable to let the proton on HO_2^- point toward W_B than towards Cu2 (H_up) by 19–91 kJ/mol. The latter structures also gave longer Cu2–Cu3/3' distances. Moreover, the {$H_2O,H_2O:A_3,HO_2^-:C_{3'}$} complex is 39–93 kJ/mol more stable than the {$H_2O,H_2O,HO_2^-:S_{23'}$} complex, providing yet another argument in favor of $C_{3'}$ binding mode also for NI'.

Likewise, if another proton is added to the O_2-derived ligand (i.e. giving H_2O_2), the O–O bond breaks automatically, and a {$L,OH,OH:S_{23},OH:S_{23'}$} structure is obtained. As can be seen in Figure 6, it has three OH^- molecules bridging each of the three pairs of copper ions. This is one of the two possible structural models for the native intermediate.[20] It gives two Cu–Cu distances of 3.26–3.44 Å (3.42 and 3.62 Å for $L = OH^-$), which are similar to that observed by EXAFS for the native intermediate, 3.3 Å.[20] The third Cu–Cu distance is ~3.9 Å. All three structures are predicted to be antiferromagnetically coupled, in agreement with the observed doublet ground state.[20] They also all have the two T3 copper ions coupled, with ~0.6 spin on the copper ions.
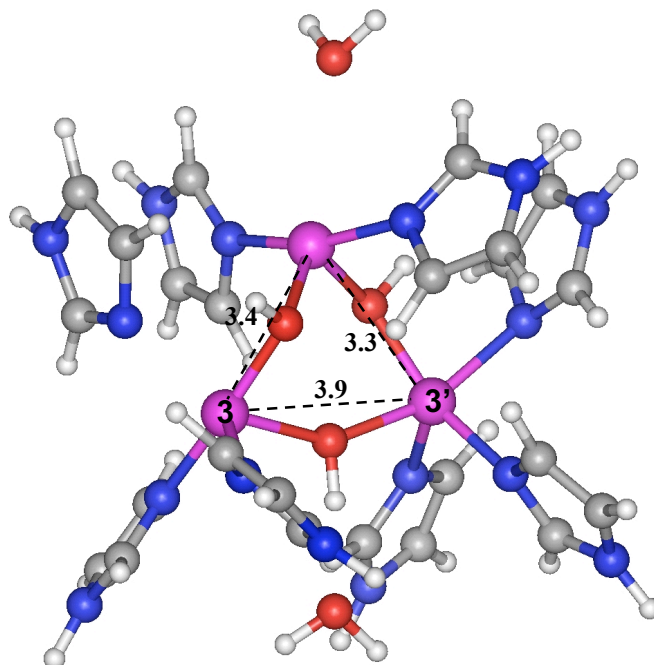
Figure 6: The $\{H_2O, OH^-, OH^-:S_{23}, OH^-:S_{23'}\}$ structure, illustrating the S_{23} binding mode of the native intermediate. L can be either H_2O as pictured or OH^-.

The alternative structural model of the native intermediate is $\{L, OH^-:A_{3/3'}, O^{2-}:C\}$.[20] We have studied six structures of this type. They always have O^{2-} in the middle of the cluster, in accordance with the suggested structure. However, we were not able to obtain an A_3 or $A_{3'}$ ligation of the B ligand (in protein, vacuum, and dielectric continuum calculations). Instead, it always moved to an almost symmetrically bridging position between the two T3 copper ions ($S_{33'}$, i.e. the normal position of the bridging ligand), as is shown in Figure 7. The six structures (with $B = O^{2-}$, OH^- or none and $L = H_2O$, OH^- or none) gave Cu–Cu distances of 2.9–3.5 Å, with averages 3.27–3.33 Å without and 3.08–3.18 Å with $B = O^{2-}$. The former are in excellent agreement with EXAFS measurements, which gave two or three Cu–Cu distances of ~3.3 Å.[20]
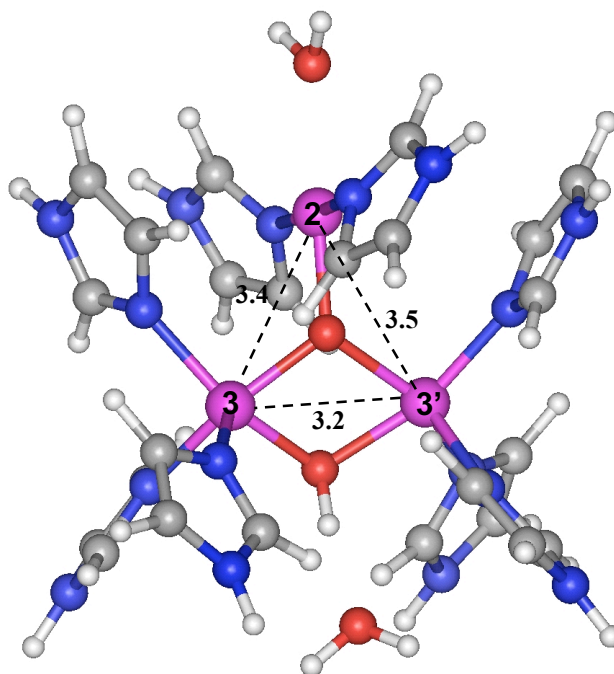
Figure 7: The {H_2O,OH^-,O^{2-}:C}structure, illustrating the C binding mode of the native intermediate.

The electronic structures of the {L,B,O^{2-}:C} structures are similar to those of the oxidized state. Thus, all three copper ions have significant spin density (0.4–0.7 e) and the antiferromagnetically coupled state is most stable for all complexes by 2–8 kJ/mol, except for {OH^-,–,O^{2-}:C} and {OH^-,H_2O,O^{2-}:C}. This is in agreement with experiments.[20] The spin coupling depends on the L ligand: If L = water or vacant, the two T3 copper ions are antiferromagnetically coupled, whereas if L = OH^-, Cu2 has a negative spin density and is therefore antiferromagnetically coupled to one of the other copper ions.

Thus, both suggested structures of the native intermediate, {L,B,O^{2-}:C} and {L,OH,OH:S_{23},OH:$S_{23'}$}, give results in good agreement with the experimental data. One possible way to discriminate between these two spectroscopic possibilities is to compare the energy between the {H_2O,OH^-,O^{2-}:C) and {–,OH^-,OH^-:S_{23},OH^-:$S_{23'}$} structures. The former is 116–143 kJ/mol more stable than the latter. In vacuum and a dielectric continuum, the difference is 42 and 6 kJ/mol, so the main difference comes from the protein, which once again seems to be too crowded for

bridging $S_{23/3'}$ ligands. Thus, our results indicate that it is likely the (O^{2-}:C) state that is observed as the native intermediate in the protein. Starting from the reduced {H_2O,–} state and allowing for a single electron and proton transfer, we would actually directly end up in the {H_2O,OH^-,O^{2-}:C) state. L can also be deprotonated to OH- in NI. It is notable that for the {L,OH^-,OH^-:S_{23},OH^-:$S_{23'}$} type of complexes, an OH^- ion has to be taken up from the surroundings during the reaction.

3.2. Reductive cleavage of O–O bond in MCOs

In the previous section, we saw that there are two different types of complexes at the level of the native intermediate, depending on whether the O–O bond is cleaved or not. Our results actually allow us to get an estimate of the activation barrier for the O-O bond cleavage reaction, starting from various structures. Thereby, we may check if the bond breakage is energetically feasible and how the energies change if the peroxide is protonated. Therefore, we have studied five possible pathways starting from the NI'{–/H_2O/OH^-,–,O_2^{2-}/HO_2^-} complexes. We assume that two electrons are transferred to O_2^{2-} concomitantly, in accordance with experimental results.[18]

The calculated reaction and activation energies are listed in the last 15 rows in Table 5. It should be noted that the energy of the transitions states were only obtained in an approximate way, viz. by a linear interpolation in Cartesian coordinates of the reactant and product QM/MM structures. Thereby, we obtain an upper estimate of the true reaction barrier. However, owing to the high similarity of the initial and final structures, these estimates are probably fairly accurate. In particular, the relative values for the five reactions should be comparable.

Several trends can be seen in Table 5. First, the reaction energies are more favorable with HO_2^- than with O_2^{2-}, especially if the (less accurate) MM energies are not included (–23 to –118 compared to –1 and 65). Likewise, HO_2^- gives a lower activation energy (78–112 kJ/mol) than O_2^{2-} (~125 kJ/mol). Third, $L = OH^-$ significantly stabilizes the product (by 50–64 kJ/mol), whereas it has a smaller effect on the activation energy (1–19 kJ/mol).

Altogether, our calculations favor the reaction from $\{-,-,O_2H^-:C_{3'}\}$ or $\{H_2O,-,O_2H^-:C_{3'}\}$, because it has the lowest activation energy (78–112 kJ/mol) and a slightly exothermic reaction energy (–38 to –68 kJ/mol). The reactions with O_2^{2-} are unlikely because they give higher activation energies and the reaction of $\{-,-,O_2^{2-}\}$ is endothermic. This indicates that protonation of the peroxide facilitates O–O bond cleavage. The calculated activation energy are reasonable in comparison with the turnover rate of the protein, 0.13–560 s^{-1},[20] corresponding to a free energy of activation of 58–79 kJ/mol.

3.3. The catalytic cycle of multicopper oxidases

It is now time to collect all the available results to discuss a detailed mechanism for the O_2 reduction by MCOs. Such a mechanism should include the protonation states of the copper ligands and the oxidation state of the cluster. One of the most important points when suggesting a detailed mechanism is the total charge of the trinuclear copper cluster. It has frequently been suggested that a metal site in the protein should have small net charge[55,56]. However, it is well established that clusters with a net charge of –2 are present in proteins, e.g. the rubredoxin active site ($Fe^{2+}Cys_4$) and structural and zinc-finger sites ($Zn^{2+}Cys_4$),[57,58,59] but such highly charged sites are strongly solvated by numerous hydrogen bonds to backbone NH groups.[57,60] In other sites with uncompensated charge in the first coordination sphere, second-sphere ligands often provide a neutralization, for example in the form of Asp/Glu–His hydrogen bonds, found in heme peroxidase, carbonic anhydrase, and coenzyme B_{12} enzymes.[61,62,63]

Regarding the trinuclear cluster in the MCOs, the cluster has a strong positive charge, +6 minus the charge on the L and B ligands in the oxidized state. As can be expected, this charge is partly compensated by carboxylate groups around the cluster. Thus, all available crystal structures of MCOs show the motif in Figure 1: There is an aspartate (Asp) group 6 Å from Cu2, which forms a hydrogen bond to the L ligand via a crystal-water molecule. Moreover, there is an Asp or a glutamate (Glu) residue 6–7 Å away from the T3 copper ions. This group forms a hydrogen bond to the B ligand via the W_B water molecule. These two hydrogen-bond networks lie at the end of two

solvent channels leading to the trinuclear cluster and providing ways in and out for oxygen, water, and protons.[11] The former group also forms a hydrogen bond to the Im group one of the Cu3 ligands, whereas the side-chain of an additional Asp residue forms a similar hydrogen bond to one of the Cu3' ligands. In fact, the total charge of a 6 Å region around trinuclear copper cluster (system 2 in our calculations) is −5, so it may compensate a quite high charge of the trinuclear copper cluster.

We will base our mechanism on the reduced structure, for which a crystal structure is available,[12] and the spectroscopic data on the PI[17] and NI.[20] From the crystal structure, it is clear that the B ligand is missing in the reduced state. We have seen in section 3.1.2. that the $\{H_2O,-\}$ protonation state fits the experimental data best. This gives a total charge of +3 for the copper cluster (quantum system), but this charge is exactly compensated by the three Asp and Glu groups mentioned above are included, illustrating the neutralizing effect of the protein.

Based on this assignment, we can now go forward. The reduced state is known to bind the O_2 molecule. In section 3.1.3., we have seen that it most likely binds in the $C_{3/3'}$ mode, thus yielding the PI$\{H_2O,-,O_2^{2-}:C_{3'}\}$ state.

Next, this intermediate will be reduced by Cu1. Following the charge arguments above, the site could then also take up a proton from the surroundings, to keep the total charge constant. As mentioned above, there are two proton-transfer paths in the protein, one ending at the T2 solvent molecule (L) and the other at the T3 bridging molecule (B). This will initially produce NI'$\{H_2O,-,HO_2^-:C_{3'}\}$ state, which is in good agreement with the results in the previous section, indicating that cleavage of the O–O bond is most favorable in this complex. The immediate product of the O–O breakage would be the NI$\{H_2O/OH^-,OH^-,O^{2-}:C\}$ state, which is also our suggested structure for the observed native intermediate (section 3.1.5).

Finally, this native intermediate should be converted to the reduced state (remember that the oxidized resting state cannot be in the catalytic cycle[20]) by the uptake of three electrons and three protons (note again the charge balance) and the dissociation of two water molecules (the products of

the reaction). This part of the reaction cycle is not yet experimentally defined and it is not considered in this article.

Thus, we have seen that our suggested structures fit nicely into a simple and lucid reaction cycle, illustrated in Figure 8. The alternative structures for the PI and NI (Figure 8) would require the binding of an extra water molecule in the O_2 reaction to form PI. This water would donate a proton to the O_2 molecule, forming the PI$\{H_2O,OH^-,HO_2^-:S_{23/3'}\}$ complex (Figure 4). After the uptake of an electron and a proton, the NI'$\{H_2O,H_2O,HO_2^-:S_{23/3'}\}$ complex would be obtained, which could reorganize to the NI$\{H_2O/OH^-,OH^-,OH^-:S_{23},OH^-:S_{23'}\}$ (Figure 6), although this reaction is appreciably more complicated than the simple O–O bond cleavage in the NI'$\{H_2O,-,HO_2^-:C_{3'}\}$ state. Finally, this complex could be converted to the reduced state by the uptake of three electrons and three protons, and the dissociation of three water molecules. Thus, we see that the alternative suggestions for the PI and NI give rise to a more complicated reaction mechanism. Moreover, we have seen that the PI$\{H_2O,OH^-,HO_2^-:S_{23/3'}\}$ and NI$\{H_2O/OH^-,OH^-,OH^-:S_{23},OH^-:S_{23'}\}$ states are energetically disfavored and show strained geometries. However, such a mechanism would explain why it is observed that the *B* ligand in the oxidized resting state is *not* derived from O_2[20] (although the *B* ligand may exchange with water during the slow conversion between the NI and the Ox state).

Ox   **Red**   **PI**
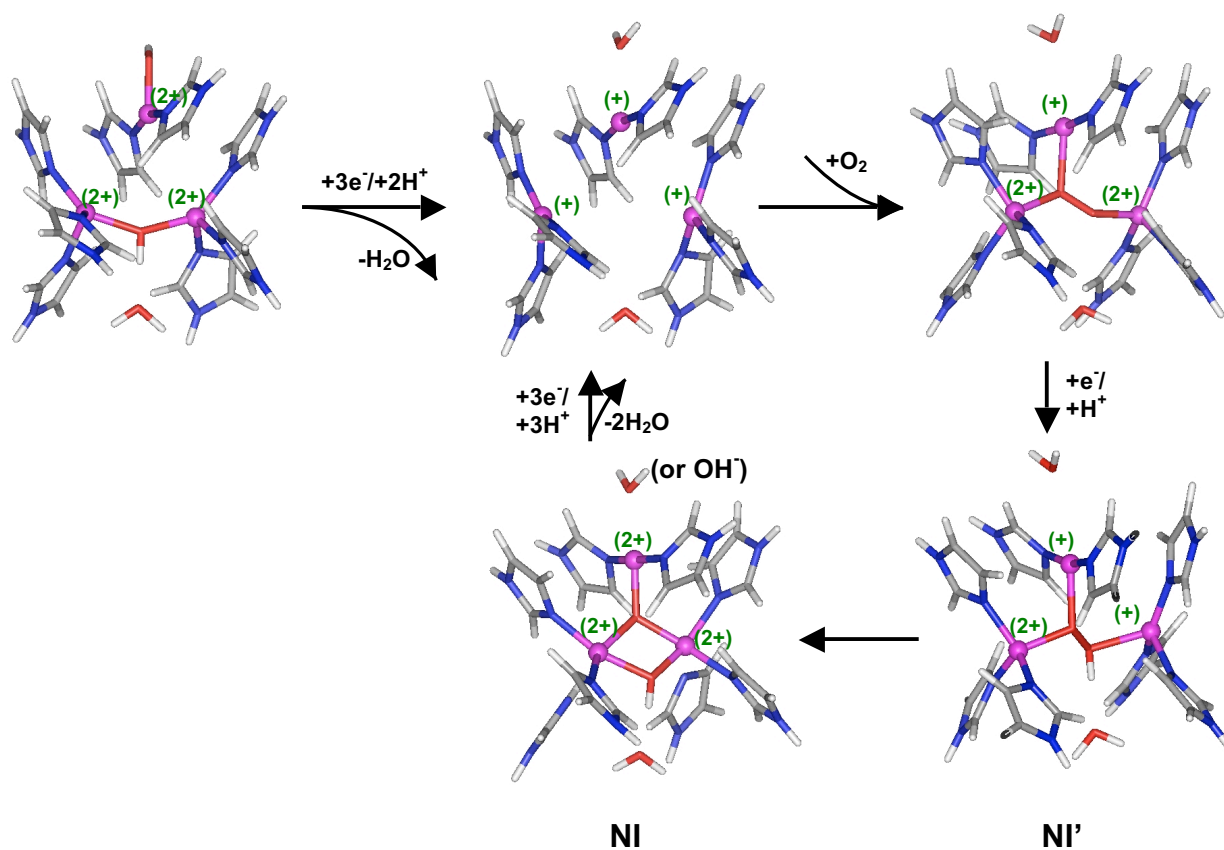
Figure 8. The suggested reaction mechanism consistent with the QM/MM calculations, spectroscopic measurements, and available crystal structures. Formal oxidation states (not necessarily corresponding to the calculated spin densities) are depicted as well.

4. Conclusions

In this investigation, we have studied five key states of the trinuclear copper cluster in the reaction cycle of MCOs using theoretical methods. The geometric and energetic data in Tables 2–5 has provided significant insight into the experimentally observed intermediates and have allowed us to suggest a reasonable reaction cycle for the O_2 reduction (Figure 8). We expect that these results will complement the extensive experimental investigations of these enzymes.

Our results indicate that the resting oxidized state of the protein is in the {OH⁻,OH⁻} protonation state and that the reduced state is {H_2O,–}, which is in accordance with experimental suggestions.[12,18,50] For the peroxy and native intermediates, spectroscopic investigations have led to

two structural interpretations for each of the states (cf. Figure 2). For the peroxy intermediate, the calculations predict that the $C_{3/3'}$ coordination mode (Figure 5) is energetically much more favorable than the $S_{23/3'}$ mode (Figure 4), which is further corroborated by a better structural agreement of the former with the experimental Cu−Cu distances. In general, it has been found that $S_{23/3'}$ structures are energetically and structurally disfavored, mainly because there is simply too little space for a bridging ligand between Cu2 and Cu3/3' and the flexibility of this region is rather limited owing to the presence of four His-X-His links. Thus, the experimentally observed PI seems to be $\{H_2O,-,O_2^{2-}:C_{3/3'}\}$. The apical (A) coordination of peroxide to one of the T3 copper ions, observed in the crystal structure of AO,[12] is not obtained in any of our geometry optimizations.

Likewise, for the native intermediate, our results show that the $\{H_2O/OH^-,OH^-,O^{2-}:C\}$ state (Figure 6) is energetically more favorable than the $\{H_2O/OH^-,OH^-,OH^-:S_{23},OH^-:S_{23'}\}$ state (Figure 7). Again, the result is mainly based on the higher stability of the former structure, owing to the lack of space between Cu2 and Cu3/3'; both structures give similar geometries and electronic structures. Moreover, the $\{H_2O/OH^-,OH^-,O^{2-}:C\}$ state also derives naturally in the reaction mechanism as the immediate product of the cleavage of the O–O bond in the NI'$\{H_2O,-,HO_2^-:C_{3/3'}\}$ intermediate. Our results also indicate that such a reaction has a reasonable activation energy of less than 80 kJ/mol.

In the interpretation of our results, it is important to take into consideration the accuracy of the theoretical method used. Our experience from the modeling of active sites of other copper proteins show that the present method should give Cu–N and Cu–Cu distances that are accurate to within 0.07 and 0.12 Å, respectively.[64,65] The stiff bonds to the negatively charged O-ligands are probably even more accurate (to within ~0.04 Å), whereas the positions of the weakly bound water molecules are determined by a delicate balance between the weak Cu–O interaction and possible hydrogen bonds to the surrounding protein, and are therefore far from reliable. Considering that the average error in crystal structures with a resolution of 1.4–2.6 Å is ~0.1 Å and that errors of over 0.3 Å are frequently found, [66,67] the QM/MM are at least as accurate as the crystal structures.

However, the estimated energies are less accurate. Density functional calculations similar to those in this paper give energies that are accurate to within ~15 kJ/mol for gas-phase processes.[68,69] However, for reactions inside a protein, the accuracy is appreciably lower. We estimate that the accuracy of the relative energies in Table 5 and the of ΔE_{spin} in Table 4 are 25 kJ/mol without and ~40 kJ/mole with the MM energies.

We have demonstrated how these intermediates, suggested by geometric and energetic criteria, give rise to a simple and consistent reaction mechanism. Throughout this mechanism, the total charge of the trinuclear copper site remains constant (at +3). This is probably important, because the surrounding protein is designed to stabilize a certain charge. It also indicates that the electron transfer may be at least partially assisted by proton transfer.

On the other hand there are two observations to be explained. First, isotope labeling indicates that the L, but not the B ligand should derive from O_2[20] in variance to the mechanism suggested in Figure 8. However, as mentioned above, there can be an exchange of the bridging ligand with water during the slow conversion of native intermediate into resting oxidized state (which does not take place under turnover conditions). Second, the $Ox\{H_2O,O^{2-}:C\}$ state seems to be more stable than the observed $Ox\{OH,OH\}$ state, yet the NI slowly decays to the resting state. However, they do not obscure our other results for the reaction cycle of MCOs, which demonstrate that theoretical methods can be used to complement experimental investigations for the study of complicated enzymes containing multinuclear metal centers to give deeper insight into their enzymatic action.

Supporting Information Available. The equilibrium geometries of all the studied molecules (or QM regions in case of QM/MM calculations) and the complete coordinates of the initial protein structure used as the model throughout this work (in PDB format) are available free of charge via the Internet at http://pubs.acs.org.

References

(1) Messerschmidt, A. In *Multicopper oxidases*; Messerschmidt, A., Ed.; World Scientific: Singapore; River Edge, NJ, 1997; pp. 23-80.

(2) Solomon, E. I.; Sundaram, U. M.; Machonkin, T. E. *Chem. Rev.* **1996**, *96*, 2563-2605.

(3) Xu, F. *Biochemistry* **1996**, *35*, 7608-7614.

(4) Davies, G. J.; Ducros, V. In *Handbook of Metalloproteins*; Messerschmidt, A., Huber, R., Wieghardt, K., Poulos, T, Eds.; Wiley, New York, 2001, pp. 1359-1368.

(5) Malkin, R.; Malmström, B. G. *Advan. Enzymol.* **1970**, *33*, 177-243.

(6) Crichton, R. R.; Pierre, J.-L. *BioMetals* **2001**, *14*, 99-112.

(7) de Silva, D.; Askwith, C. C.; Eide, D.; Kaplan, J. *J. Biol. Chem.* **1995**, *270*, 1098-1101.

(8) Outten, F. W.; Huffman, D. L.; Hale, J. A.; O'Halloran, T. V. *J. Biol. Chem.* **2001**, *276*, 30670-30677.

(9) Piontek, K.; Antorini, M.; Choinowski, T. *J. Biol. Chem.* **2002**, *277*, 37663-37669.

(10) Bertrand, T.; Jolivalt, C.; Briozzo, PI.; Caminade, E.; Joly, NI.; Madzak, C.; Mougin, C. *Biochemistry* **2002**, *41*, 7325-7333.

(11) Messerschmidt, A.; Ladenstein, R.; Huber, R; Bolognesi, M.; Avigliano, L; Petruzzelli, R.; Rossi, A.; Finazzi-Agro, A. *J. Mol. Biol.* **1992**, *224*, 179-205.

(12) Messerschmidt, A.; Luecke, H.; Huber, R. *J. Mol. Biol.* **1993**, *230*, 997-1014.

(13) Hakulinen, NI.; Kiiskinen, L.-L.; Kruus, K.; Saloheimo, M.; Paananen, A.; Koivula, A.; Rouvinen, J. *NI. Struct. Biol.* **2002**, *9*, 601-605.

(14) Enguita, F. J.; Martins, L. O.; Henriques, A. O.; Carrondo, M. A. *J. Biol. Chem.* **2003**, *278*, 19416-19425.

(15) (a) Roberts, S. A.; Weichsel, A.; Grass, G.; Thakali, K; Hazzard, J. T.; Tollin, G.; Rensing, C.; Montfort, W. R. *Proc. Natl. Acad. Sci. U.S.A.* **2002**, *99*, 2766-2771. (b) Roberts, S. A.; Wildner, G. F.; Grass, G.; Weichsel, A.; Ambrus, A.; Rensing, C.; Montfort, W. R. *J. Biol. Chem.* **2003**, *278*, 31958-31963.

(16) Berman, H. M.; Westbrook, J.; Feng, Z.; Gilliland, G.; Bhat, T. NI.; Weissig, H.; Shindyalov, I. NI.; Bourne, PI. E. *Nucleic Acids Research*, **2000,** *28*, 235-242.

(17) Shin, W.; Sundaram, U. M.; Cole, J. L.; Zhang, H. H.; Hedman, B; Hodgson, K. O.; Solomon, E. I. *J. Am. Chem. Soc.* **1996**, *118*, 3202-3215.

(18) Palmer, A. E.; Lee, S.-K.; Solomon, E. I. *J. Am. Chem. Soc.* **2001**, *123*, 6591-6599.

(19) Palmer, A. E.; Quintanar, L.; Severance, S.; Wang, T.-PI.; Kosman, D. J.; Solomon, E. I. *Biochemistry* **2002**, *41*, 6438-6448.

(20) Lee, S.-K.; George, S. D.; Antholine, W. E.; Hedman, B; Hodgson, K. O.; Solomon, E. I. *J. Am. Chem. Soc.* **2002**, *124*, 6180-6193.

(21) Torres, J.; Svistunenko, D.; Karlsson, B.; Cooper, C. E.; Wilson, M. T. *J. Am. Chem. Soc.* **2002**, *124*, 963-967.

(22) Solomon, E. I.; Chen, PI.; Metz, M.; Lee, S.-K.; Palmer, A E. *Angew. Chem. Int. Ed.* **2001**, *40*, 4570-4590.

(23) Olsson, M. H. M.; Ryde, U. *J. Am. Chem. Soc.* **2001**, *123*, 7866-7876.

(24) Metz, M.; Solomon, E. I. *J. Am. Chem. Soc.* **2001**, *123*, 4938-4950.

(25) Siegbahn, PI. E. M. *J. Biol. Inorg. Chem.* **2003**, *8*, 567-576.

(26) Henson, M. J.; Vance, M. A.; Zhang, C. X.; Liang, H. C.; Karlin, K. D.; Solomon, E. I. *J. Am. Chem. Soc.* **2003**, *125*, 5186-5192.

(27) Ryde, U. *J. Comput.-Aided Mol. Design* **1996**, *10*, 153-164.

(28) Ryde, U.; Olsson, M. H. M. *Int. J. Quantum Chem.* **2001**, *81*, 335-347.

(29) Treutler, O.; Ahlrichs, R. *J. Chem. Phys.* **1995**, *102*, 346-354.

(30) Case, D. A.; Pearlman, D. A.; Caldwell, J. W.; Cheatham III, T. E.; Wang, J.; Ross, W. S.; Simmerling, C. L.; Darden, T. A.; Merz, K. M.; Stanton, R. V.; Cheng, A. L.; Vincent, J. J.; Crowley, M.; Tsui, V.; Gohlke, H.; Radmer, R. J.; Duan, Y.; Pitera, J.; Massova, I.; Seibel, G. L.; Singh, U. C.; Werner, PI. K.; Kolman, PI.. A. AMBER 7, University of California, San Francisco, 2002.

(31) Cornell, W. D.; Cieplak, PI.; Bayly, C. I.; Gould, I. R.; Merz, K. M.; Ferguson, D. M.; Spellmeyer, D. C.; Fox, T.; Caldwell, J. W.; Kolman, PI.. A. *J. Am. Chem. Soc.* **1995**, *117*, 5179-5197.

(32) Reuter, NI.; Dejaegere, A.; Maigret, B.; Karplus, M. *J. Phys. Chem.* **2000**, *104*, 1720-1735.

(33) Svensson, M.; Humbel, S.; Froese, R. D. J.; Matsubara, T.; Sieber, S.; Morokuma, K. *J. Phys. Chem.* **1996**, *100*, 19357-19363.

(34) Ryde, U.; Olsen, L.; Nilsson, K. *J. Comput. Chem.* **2002**, *23*, 1058-1070.

(35) Titmuss, S. J.; Cummins, PI. L.; Bliznyuk A. A.; Rendell, A. PI.; Gready, J. E. *Chem. Phys. Lett.* **2000**, *320*, 169-176.

(36) (a) Becke, A. D. *Phys. Rev. A* **1988**, *38*, 3098-3100. (b) Perdew, J. PI. *Phys. Rev. B* **1986**, *33*, 8822-8824.

(37) Eichkorn, K.; Treutler, O.; Öhm, H.; Häser, M.; Ahlrichs, R. *Chem. Phys. Lett.* **1995**, *240*, 283-290.

(38) Eichkorn, K.; Weigen, F.; Treutler, O.; Ahlrichs, R. *Theor. Chim. Acta* **1997**, *97*, 119-124.

(39) Schäfer, A.; Huber, C.; Ahlrichs, R. *J. Chem. Phys.* **1994**, *100*, 5829-5835.

(40) Hehre, W. J.; Radom, L.; Schleyer, PI. v. R.; Pople, J. A. *Ab initio molecular orbital theory*; Wiley-Interscience: New York, 1986.

(41) Becke, A. D. *J. Chem. Phys.* **1993**, *98*, 5648.

(42) Hertwig, R. H.; Koch W. *Chem. Phys. Lett.* **1997**, *268*, 345.

(43) (a) Krishnan, R.; Binkley, J. S.; Seeger, R.; Pople, J. A. *J. Chem. Phys.* **1980**, *72*, 650. (b) Clark, T.; Chandrasekhar, J.; Schleyer, P. v. R. *J. Comput. Chem.* **1983**, *4*, 294.

(44) Because we have used the unrestricted Kohn-Sham (KS) formalism, the resulting KS determinants are not eigenfunctions of the $\hat{S}^2$ operator. While the deviation from the pure $S = 3/2$ (or $S = 1$ for peroxy) states is negligible for the ferromagnetically coupled states, the antiferromagnetically coupled states deviate significantly from pure $S = 1/2$ (or $S = 0$) states, which can only be described by multireference wave functions. Nevertheless, this approach is routinely used in the studies of antiferromagnetically coupled model complexes representing metal sites in proteins. The reported values are unrestricted DFT energies without spin projection. The broken-symmetry technique can be used to correct the energies of the antiferromagnetically coupled (AF) states, viz. $E_{AF} = E_F - 3/2(E_F - E_{BS})$ for all three coppers coupled and $E_{AF} = E_F - 2(E_F - E_{BS})$ for two coppers coupled (e.g., peroxy intermediate), where E_F and E_{BS} are the energies of the feromagnetically coupled state and the broken symmetry solution of the AF state, respectively, whereas E_{AF} is the corrected energy of the AF state.

(45) Noodleman, L.; Peng, C. Y.; Case, D. A.; Mouesca, J.-M. *Coord. Chem. Rev.* **1995**, *144*, 199-244.

(46) Klamt, A.; Schuurmann, G. *J. Chem. Soc.-Perkin Trans. 2* **1993**, 799-805.

(47) Schäfer, A.; Klamt, A.; Sattel, D.; Lohrenz, J. C. W.; Eckert, F. *Phys. Chem. Chem. Phys.* **2000**, *2*, 2187-2193.

(48) Klamt, A.; Jonas, V.; Bürger, T.; Lohrenz, J. C. W. *J. Phys. Chem. A* **1998**, *102*, 5074-5085.

(49) Cole, J. L.; Clark, P. A.; Solomon, E. I. *J. Am. Chem. Soc.* **1990**, *112*, 9534-9548.

(50) Quintanar, L.; Solomon, E. I., *to be published*.

(51) Barone, V.; Bencini, A.; Ciofini, I.; Daul, C. A.; Totti, F. *J. Am. Chem. Soc.* **1998**, *120*, 8357.

(52) Andersson, K.; Malmqvist, P.-Å.; Roos, B. O. *J. Chem. Phys.* **1992**, *96*, 1218.

(53) Rulíšek, L.; Neese, F.; Solomon, E. I.; Ryde U. *manuscript in preparation*.

(54) Sundaram, U. M.; Zhang, H. H.; Hedman, B.; Hodgson, K. O.; Solomon, E. I. *J. Am. Chem. Soc.* **1997**, *119*, 12525-12540.

(55) Lippard, S. J.; Berg, J. M. *Principles of bioinorganic chemistry*, University Science Books, Mill Valley, USA, 1994.

(56) Siegbahn, P. E. M.; Blomberg, M. R. A. *Chem. Rev.* **2000**, *100*, 421-437.

(57) Ryde, U. *Eur. Biophys. J.* **1996**, *24*, 213-221.

(58) Dudev, T; Lim, C. *J. Am. Chem. Soc.* **2002**, *124*, 6759-6766.

(59) Sigfridsson, E.; Olsson, M. H. M.; Ryde, U. *Inorg. Chem.* **2001**, *40*, 2509-2519.

(60) Adman, E. T.; Watenpaugh, K. D.; Jensen, L. H. *Proc. Natl. Acad. Sci. U.S.A.* **1975,** *72*, 4854-4858.

(61) Gajhede, M. **2001** in Handbook of metalloproteins (Messerschmidt, A; Huber, R.; Poulos, T.; Wieghart, K., eds), Whiley, Chichester, pp. 233-244.

(62) Gruber, K.; Kratky, C. **2001** in Handbook of metalloproteins (Messerschmidt, A; Huber, R.; Poulos, T.; Wieghart, K., eds), Whiley, Chichester, pp. 995-1009.

(63) Lindskog, S. *Pharmacol. Ther.* **1997**, *74*, 1-20.

(64) Olsson, M. H. M; Ryde, U. *J. Am. Chem. Soc.* **2001**, *123*, 7866-7876.

(65) Ryde, U.; Olsson, M. H. M. *Int. J. Quanum Chem.* **2001***, 81*, 335-347.

(66) Ryde, U.; Nilsson, K. *J. Mol. Struct. (THEOCHEM)* **2003**, *632*, 259-275.

(67) Ryde, U.; Nilsson, K. *J. Am. Chem. Soc.* **2003**, *125*, 14232-14233.

(68) Curtiss, L. A.; Raghavachari, K.; Redrern, P. C.; Pople, J.A. *J. Chem. Phys.* **1997**, *106*, 1063-1079.

(69) Curtiss, L. A.; Raghavachari, K.; Redrern, P. C.; Pople, J.A. *J. Chem. Phys.* **2000**, *112*, 7374-7383.

Table 1. A summary of all three-dimensional structures of multicopper oxidases (containing the full complement of copper ions) deposited in the PDB. All distances are in Å. The distances r_{23}, $r_{23'}$, and $r_{33'}$ are between the three copper ions, the r_{2L} distance is between Cu2 and its coordinated solvent molecule, whereas r_{3B} and $r_{3'B}$ are the distances between Cu3 or Cu3' and the bridging solvent molecule (or peroxide, O_2, N_3^-, Cl^-). $\alpha_{3B3'}$ is the angle between Cu3, bridging ligand (if present) and Cu3'.

PDB code	Resol. (Å)	Redox State	Enzyme	Source	r_{23}	$r_{23'}$	$r_{33'}$	r_{2L}	r_{3B}; $r_{3'B}$	Ref	$\alpha_{3B3'}$	Comments
1GYC	1.9	oxidized	laccase	*Trametes versicolor*	3.81	3.81	3.91	2.35	2.08; 2.19	9	152	
1KYA	2.4	oxidized	Laccase with 2,5-xylidine	*Trametes versicolor*	3.89	3.85	3.91	2.40	1.90; 2.07	10	162	
1AOZ	1.9	oxidized	AO	*Zucchini*	3.79	3.84	3.71	2.03	2.03; 2.00	11	135	
1ASO	2.2	reduced	AO	*Zucchini*	4.08	4.44	5.11	2.18	–	12	–	
1ASP	2.59	oxidized	AO with peroxide	*Zucchini*	3.77	4.45	4.80	2.06	1.94; 3.95	12	–	HO_2^- bound to Cu3
1ASQ	2.32	reduced	AO with azide	*Zucchini*	3.61	4.64	5.10	2.08	1.97; 3.14	12	–	N_3^- bound to Cu3
1GW0	2.4	partially reduced	Laccase	*Melanocarpus albomyces*	3.89	4.05	4.83	2.48	2.45; 2.54	13	–	$L = Cl^-$ and $B = O_2$
1GSK	1.7	partially reduced	CotA	*Bacillus subtilis*	4.64	4.67	4.28	2.07	2.11; 2.19	14	168	Cu2 trigonal
1KV7	1.4	partially reduced	CueO	*Escherichia coli*	3.54	3.98	4.70	2.96	2.29; 2.43	15a	170	
1N68	1.7	partially reduced	CueO with regulatory Cu ion	*Escherichia coli*	3.62	4.09	4.80	2.94	2.31; 2.50	15b	176	
1PF3	1.5	partially reduced	CueO M441L mutant	*Escherichia coli*	3.75	4.17	4.84	2.79	2.39; 2.46	15b	171	

Table 2. The optimized QM/MM geometries of the oxidized and reduced states of CueO. The distances r_{23}, $r_{23'}$, and $r_{33'}$ are between the copper ions, the r_{2L} distance is between Cu2 and its coordinated solvent molecule, whereas r_{3B}, $r_{3'B}$ and r_{2B} are the distances between Cu3, Cu3', or Cu2 and the bridging solvent molecule (the r_{2B} distance is included only if B is in the center of Cu$_3$ triangle, B:C). All distances are in Å. Finally, $\alpha_{3B3'}$ is the Cu3–B–Cu3' angle (in degrees). It has a positive (negative) value, if bridging oxygen atom is located outside (inside) Cu$_3$ triangle.

Ox State	Protonation State	Cu–Cu			Cu2–L	Cu3–B		Cu–N_{Im} distances		
		r_{23}	$r_{23'}$	$r_{33'}$	r_{2L}	r_{3B}; $r_{3'B}$; r_{2B}	$\alpha_{3B3'}$	Cu2	Cu3	Cu3'
Oxidized	{OH⁻,H$_2$O}	4.26	4.90	5.37	1.87	2.14;3.32	153	1.89;1.94	1.94;1.96;1.97	1.93;1.93;1.99
	{H$_2$O,OH⁻}	3.82	4.23	3.83	2.12	1.95;1.99	155	1.90;1.91	1.99;2.02;2.04	2.00;2.01;2.04
	{OH⁻,OH⁻}	3.86	4.11	3.75	1.87	1.94;1.97	147	1.88;1.93	2.00;2.01;2.05	2.01;2.02;2.03
	{H$_2$O,O²⁻:C}	3.22	3.39	3.39	2.57	1.88;1.91(2.00)	−127	1.92;1.93	2.00;2.00;2.13	2.01;2.03;2.03
	{OH⁻,O²⁻:C}	3.15	3.24	3.49	1.87	1.90;1.92(1.90)	−132	1.94;1.93	2.03;2.04;2.11	2.02;2.03;2.08
	{OH⁻,OH:S$_{23}$}	3.36	4.12	4.78	1.84	2.03;1.92	−116	1.97;1.99	1.95;2.01;2.05	1.91;1.92;1.98
	{−,OH⁻,OH:S$_{23'}$}	3.34	3.75	3.72	−	1.95;1.98	142	1.89;1.91	2.01;2.02;2.05	2.00;2.09;2.22
Reduced	{H$_2$O,−}	4.00	4.34	5.22	2.62	−	−	1.87;1.87	1.94;1.95;1.98	1.93;1.94;2.03
	{OH⁻,−}	4.24	4.57	5.25	1.94	−	−	1.91;1.96	1.93;1.94;1.99	1.93;1.94;2.04
	{−,H$_2$O}	3.57	4.29	5.22	−	2.31;2.99	159	1.87;1.87	1.96;1.97;2.04	1.94;1.94;2.05
	{H$_2$O,H$_2$O}	3.88	4.21	4.97	2.75	2.32;2.72	161	1.87;1.88	1.96;1.97;2.04	1.95;1.96;2.05
	{OH⁻,H$_2$O}	4.00	4.40	5.22	1.96	2.27;3.00	164	1.92;1.95	1.95;1.97;2.03	1.94;1.95;2.04
	{H$_2$O,OH⁻:C}	2.75	2.92	4.29	3.94	2.12;2.22(2.05)	161	1.94;1.97	1.98;2.03;2.07	1.96;2.01;2.12
	{OH⁻,OH⁻}	4.13	4.47	4.01	1.93	2.01;2.06	161	1.93;2.07	1.97;2.08;2.14	1.97;2.05;2.12
	{−,H$_2$O,OH:S$_{23'}$}	3.67	3.97	5.24	2.04;2.13	2.12;3.54	133	1.91;1.93	1.97;1.98;2.08	1.96;2.01;2.09

Table 3. The equilibrium geometries resulting from the QM/MM calculations for peroxy (PI), native (NI) intermediate and peroxy adduct (PA) of CueO. All distances are in Å, angles in degrees. For the abbreviations, see the legend of Table 2.

Ox State	Protonation State	Cu–Cu			L	Cu3–B		O-O	Cu–O$_2$	Cu–N$_{Im}$ distances		
		r_{23}	$r_{23'}$	$r_{33'}$	r_{2L}	r_{3B}; $r_{3'B}$	$\alpha_{3B3'}$	$r(O_1\text{-}O_2)$		Cu2	Cu3	Cu3'
PI	{−,−,O$_2^{2-}$:C$_{3'}$}	3.52	3.88	4.65	−	−	−	1.34	1.98;1.98;2.19[d]	1.88;1.88	1.99;2.00;2.01	1.98;2.01;2.04
	{H$_2$O,−,O$_2^{2-}$:C$_3$}	3.55	3.76	4.60	3.04	−	−	1.35	2.03;1.94;2.15	1.90;1.91	2.00;2.01;2.01	1.97;1.99;2.04
	{H$_2$O,−,O$_2^{2-}$:C$_{3'}$}	3.57	3.93	4.61	3.00	−	−	1.34	1.98;1.98;2.23[d]	1.88;1.89	1.99;2.00;2.01	1.98;2.01;2.03
	{OH$^-$,−,O$_2^{2-}$:C$_{3'}$}	3.45	3.95	4.54	1.92	−	−	1.39	2.02;1.99;2.02[d]	1.97;1.99	2.00;2.00;2.04	1.99;2.00;2.05
	{H$_2$O,H$_2$O:A$_3$,O$_2^{2-}$:C$_{3'}$}	3.67	4.13	4.58	2.53	2.25;3.55	102	1.38	2.02;2.03;2.12	1.93;1.93	2.03;2.09;2.12	1.98;2.01;2.05
	{H$_2$O,OH$^-$:A$_3$,O$_2^{2-}$:C$_{3'}$}	3.59	3.94	4.45	3.02	1.90;3.93	92	1.37	1.99;1.98;2.09	1.90;1.91	2.13;2.17;2.26	1.97;2.03;2.04
	{−,−,HO$_2^-$:C$_{3'}$}	3.48	3.92	5.11	−	−	−	1.44	1.95;2.31;2.10	1.90;1.91	1.95;1.98;1.99	1.98;1.98;1.99
	{H$_2$O,−,HO$_2^-$:C$_{3'}$}	3.54	4.05	5.07	2.78	−	−	1.44	2.15;1.96;2.31	1.91;1.92	1.99;1.98;1.96	1.99;1.96;1.99
	{H$_2$O,−,HO$_2^-$:C$_{3'}$} H_up	4.13	4.31	4.94	2.43	−	−	1.43	2.76;2.29;1.95	1.90;1.92	1.93;1.95;1.98	2.00;2.00;2.01
	{OH$^-$,−,HO$_2^-$:C$_{3'}$}	3.52	4.11	4.97	1.91	−	−	1.47	2.13;1.99;2.18	1.95;1.95	1.98;1.99;2.01	1.98;1.99;2.03
	{H$_2$O,OH$^-$,O$_2^{2-}$:S$_{23}$}	3.37	2.87	4.12	2.86	2.06;2.10	165	1.34	2.07;2.08[a]	1.95;1.95	2.13;2.13;2.15	2.05;2.06;2.14
	{H$_2$O,OH$^-$,O$_2^{2-}$:S$_{23'}$}	3.42	4.16	3.83	2.49	2.01;2.05	141	1.35	2.00;1.98	1.95;1.98	2.02;2.05;2.13	2.07;2.16;2.27
	{H$_2$O,OH$^-$,HO$_2^-$:S$_{23}$}	3.64	2.76	3.91	3.31	2.06;1.98	151	1.44	1.99;1.94[a]	1.98;2.03	2.01;2.10;2.13	2.06;2.06;2.10
	{H$_2$O,OH$^-$,HO$_2^-$:S$_{23'}$}	3.78	4.63	3.53	2.28	1.93;1.97	130	1.45	1.95;2.78 2.88;2.14[b]	2.00;2.00	2.06;2.06;2.11	2.03;2.10;2.21
	{OH$^-$,OH$^-$,HO$_2^-$:C$_\perp$} H_up	4.50	4.93	3.34	1.79	1.95;1.95	117	1.46	2.08;3.07 3.22;2.04[b]	1.94;**3.43**	2.05;2.13;2.18	2.06;2.18;2.18
	{H$_2$O,OH$^-$,OH$^-$:S$_{23}$,OH$^-$:S$_{23'}$}	4.44	4.04	3.64	2.11	1.93;2.02	135	**2.69**	1.81;3.73;101 2.09;1.97;168[c]	1.96;1.97	1.93;1.97;2.69	2.00;2.05;2.13
PA	{OH$^-$,−,O$_2^{2-}$:C$_3$}	3.66	3.76	4.56	1.88	−	−	1.35	2.11;1.95;2.03	1.94;1.96	2.00;2.00;2.00	1.97;1.97;2.03
	{OH$^-$,−,O$_2^{2-}$:C$_{3'}$}	3.52	4.13	4.55	1.88	−	−	1.36	2.05;1.97;2.01	1.93;1.93	2.01;2.01;2.02	1.98;1.99;2.04
	{OH$^-$,H$_2$O:A$_3$,O$_2^{2-}$:C$_3$}	3.88	3.88	4.58	1.87	3.34;2.07	63	1.37	2.23;1.99;1.99	1.95;1.96	1.99;1.99;2.03	2.01;2.05;2.13
	{OH$^-$,OH$^-$,HO$_2^-$:S$_{23'}$}	3.72	4.03	3.72	1.88	1.94;1.98	144	1.45	2.12;2.01	1.98;2.00	2.02;2.05;2.07	2.06;2.06;2.20
	{OH$^-$,OH$^-$,HO$_2^-$:C$_\perp$} H_up	3.88	4.65	3.02	1.88	2.02;1.95	99	1.46	2.59;2.03;2.07	1.95;1.97	2.01;2.09;2.25	1.97;2.05;**3.55**
NI'	{−,−,O$_2^{2-}$:C$_{3'}$}	3.28	3.95	4.55	−	−	−	1.42	1.99;1.96;2.07	1.91;1.92	2.01;2.02;2.05	2.00;2.01;2.06
	{H$_2$O,−,O$_2^{2-}$:C$_{3'}$}	3.27	3.90	4.63	3.24	−	−	1.41	1.99;1.96;2.07	1.91;1.91	2.01;2.03;2.04	1.99;2.02;2.05

{OH⁻,–,O₂²⁻:C₃'}	3.34	3.97	4.55	1.96	–	–	1.45	2.00;1.97;2.02	1.91;2.01	2.03;2.03;2.05	1.97;2.02;2.10
{–,–,HO₂⁻:C₃'}	3.36	3.76	4.70	–	–	–	1.46	1.97;2.14;2.20	1.90;1.90	1.99;1.99;2.01	1.97;1.98;2.07
{–,–,HO₂⁻:C₃'} H_up	3.99	4.11	4.94	–	–	–	1.46	2.29;1.93;2.43	1.88;1.89	1.95;1.98;1.99	2.00;2.01;2.02
{H₂O,–,HO₂⁻:C₃'}	3.39	3.74	4.75	3.28	–	–	1.47	1.97;2.17;2.16	1.90;1.91	1.99;1.99;2.01	1.97;1.98;2.07
{H₂O,–,HO₂⁻:C₃'} H_up	4.01	4.68	4.67	2.26	–	–	1.45	2.12;1.95;3.01	1.92;1.92	1.99;2.00;2.01	1.97;2.01;2.04
{OH⁻,–,HO₂⁻:C₃'}	3.50	4.17	4.93	1.92	–	–	1.54	2.01;2.16;2.03	1.96;1.96	1.99;2.00;2.02	1.95;1.96;2.06
{OH⁻,–,HO₂⁻:C₃'} H_up	4.07	4.51	4.76	1.91	–	–	1.45	2.10;1.96;2.97	1.94;1.96	1.99;1.99;2.00	1.99;1.99;2,08
{H₂O,OH⁻,HO₂⁻:S₂₃'}	3.01	3.79	3.81	2.96	1.98;2.03	145	1.48	2.05;2.00[a]	1.97;1.99	2.01;2.10;2.12	2.09;2.10;2.34
NI {–,OH⁻,OH⁻:S₂₃,OH⁻:S₂₃'}	3.44	3.26	3.90	–	2.02;2.06	146		1.88;1.95;128 1.88;2.05;112[c]	1.99;2.00	1.98;2.14;2.16	1.97;2.17;2.25
{H₂O,OH⁻,OH⁻:S₂₃,OH⁻:S₂₃'}	3.41	3.27	3.93	3.18	2.01;2.08	148		1.91;1.94;125 1.88;2.03;113[c]	1.99;1.99	2.00;2.14;2.17	1.96;2.17;2.26
{OH⁻,OH⁻,OH⁻:S₂₃,OH⁻:S₂₃'}	3.42	3.75	3.62	1.89	1.99;2.03	128		1.91;1.99;123 1.90;2.20;133[c]	2.07;2.08	1.99;2.17;2.23	2.04;2.18;2.32
{H₂O,–,O²⁻:C}	3.22	3.39	3.39	2.57	–	–		2.01;1.88;1.90	1.92;1.93	2.00;2.00;2.13	2.01;2.03;2.03
{OH⁻,–,O²⁻:C}	3.15	3.24	3.49	1.87	–	–		1.96;1.89;1.89	1.94;1.93	2.03;2.04;2.11	2.02;2.03;2.08
{OH⁻,H₂O,O²⁻:C}	3.30	3.40	3.36	1.86	2.15;2.28	99		1.86;1.99;1.99	1.94;1.96	2.04;2.13;2.13	2.07;2.17;2.24
{H₂O,H₂O,O²⁻:C}	3.32	3.53	3.32	2.25	2.18;2.09	102		1.93;1.98;1.99	1.94;1.95	2.02;2.07;2.16	2.01;2.18;2.21
{–,OH⁻,O²⁻:C}	3.26	3.42	3.16	–	1.92;1.99	108		1.90;2.00;1.93[e]	1.91;1.93	2.00;2.07;2.25	2.05;2.13;2.21
{H₂O,OH⁻,O²⁻:C}	3.36	3.48	3.15	2.37	1.91;1.97	108		1.92;1.92;2.04[e]	1.94;1.95	2.02;2.05;2.27	2.03;2.19;2.22
{OH⁻,OH⁻,O²⁻:C}	3.25	3.45	3.11	1.89	1.97;1.98	104		1.98;1.96;1.88[e]	1.98;2.01	2.06;2.09;2.31	2.08;2.19;2.28
{–,O²⁻,O²⁻:C}	3.13	3.12	3.00	–	1.84;1.93	105		1.99;1.87;1.99[e]	1.95;1.97	1.98;2.06;**2.67**	2.06;2.09;2.29
{OH⁻,O²⁻,O²⁻:C}	3.27	3.35	2.93	1.91	1.91;1.90	101		1.91;1.94;1.97[e]	2.00;2.03	2.08;2.31;2.33	2.12;2.18;2.40

[a] The reported distances are $r(O_A–Cu_3)$, $r(O_A–Cu_2)$

[b] The reported distances are $r(O_A–Cu_{3'})$, $r(O_A–Cu_2)$, {$r(O_B–Cu_{3'})$, $r(O_B–Cu_2)$

[c] The reported distances are $r(O_A–Cu_{3'})$, $r(O_A–Cu_2)$, α_{2B3}, {$r(O_B–Cu_{3'})$, $r(O_B–Cu_2)$, $\alpha_{2B3'}$

[d] O_A of O_2^{2-} is bridging the (Cu₂,Cu₃) pair, whereas O_B is coordinated to Cu₃'. The values correspond to $r(O_A–Cu_3)$, $r(O_B–Cu_{3'})$, $r(O_A–Cu_2)$

[d'] O_A of O_2^{2-} is bridging the (Cu₂,Cu₃') pair, whereas O_B is coordinated to Cu₃. The values correspond to $r(O_A–Cu_3)$, $r(O_B–Cu_{3'})$, $r(O_A–Cu_2)$

[e] The three reported distances are $r(O–Cu_3)$, $r(O–Cu_{3'})$, $r(O–Cu_2)$

Table 4. Calculated spin densities for copper ions and O-ligands in the QM/MM structures. Both the ferro- and antiferromagnetically coupled states are listed. All values were obtained at the B3LYP/6–311++G(2d,2p) level. The protein environment was represented by point charges. ΔE_{spin} is the energy difference between the ferro- and antiferromagnetically coupled states (without any MM term), with a positive sign indicating that the latter state is most stable.

Redox state	State	Total Spin	Cu2	Cu3	Cu3'	O_L	O_B	$O(O_2)$	ΔE_{spin} (kJ/mol)
Ox	$\{OH^-,H_2O\}$	1/2	0.54	0.72	−0.76	0.42	0.02		0.5
		3/2	0.54	0.72	0.77	0.43	0.02		
	$\{H_2O,OH^-\}$	1/2	−0.63	0.80	0.77	−0.03	0.15		0.8
		3/2	0.65	0.76	0.77	0.03	0.14		
	$\{OH^-,OH^-\}$	1/2	0.50	0.70	−0.68	0.40	0.00		11.3
		3/2	0.51	0.78	0.78	0.40	0.16		
	$\{H_2O,O^{2-}\}$	1/2	0.61	0.65	−0.70	0.01	0.34		9.2
		3/2	0.60	0.71	0.75	0.01	0.50		
	$\{OH^-,O^{2-}\}$	1/2	−0.39	0.54	0.54	−0.13	0.34		−22.6
		3/2	0.59	0.72	0.63	0.18	0.51		
PI	$\{-,-,O_2^{2-}:C_3\}$	0	−0.04	−0.32	0.31	–	–	0.06	−17.9
		1	0.04	0.28	0.32	–	–	1.22	
	$\{H_2O,-,O_2^{2-}:C_3\}$	0	−0.08	−0.14	0.32	0.00	–	−0.09	−20.5
		1	0.06	0.27	0.31	0.00	–	1.24	
	$\{H_2O,-,O_2^{2-}:C_{3'}\}$	0	0.02	0.20	−0.38	0.00	–	0.17	−17.2
		1	0.10	0.27	0.30	0.00	–	1.16	
	$\{OH^-,-,O_2^{2-}:C_{3'}\}$	0	0.54	−0.10	−0.21	0.13	–	−0.46	−6.2
		1	0.50	0.14	0.20	0.13	–	0.83	
	$\{H_2O,OH^-:A_3,O_2^{2-}:C_{3'}\}$	0	0.00	0.50	−0.20	0.00	0.20	−0.57	−12.9
		1	0.04	0.54	0.21	0.00	0.18	0.90	
	$\{-,-,HO_2^-:C_{3'}\}$	0	−0.03	−0.61	0.69	–	–	0.11	−4.7
		1	0.18	0.65	0.61	–	–	0.27	
	$\{H_2O,-,HO_2^-:C_{3'}\}$	0	−0.40	−0.01	0.45	0.00	–	−0.12	−20.0
		1	0.32	0.52	0.53	0.00	–	0.37	
	$\{H_2O,-,HO_2^-:C_{3'}\}$ H_up	0	−0.05	−0.69	0.56	0.00	–	0.31	4.6
		1	0.05	0.69	0.56	0.00	–	0.35	
	$\{OH^-,-,HO_2^-:C_{3'}\}$	0	−0.57	0.46	0.13	−0.20	–	0.21	−0.5
		1	0.57	0.49	0.16	0.21	–	0.32	
	$\{H_2O,OH^-,O_2^{2-}:S_{23}\}$	0	0.07	−0.51	−0.11	0.00	−0.09	0.72	−9.3
		1	0.08	0.48	0.11	0.00	0.09	1.16	
	$\{H_2O,OH^-,O_2^{2-}:S_{23'}\}$	0	0.20	-0.11	-0.45	0.00	-0.14	0.48	-10.3
		1	0.14	0.04	0.53	0.00	0.10	1.09	
	$\{H_2O,OH^-,HO_2^-:S_{23}\}$	0	−0.07	0.58	−0.54	0.00	−0.08	0.08	0.2
		1	0.25	0.62	0.43	0.00	0.16	0.28	
	$\{H_2O,OH^-,HO_2^-:S_{23'}\}$	0	0.01	−0.60	0.54	0.00	−0.02	0.09	9.2
		1	0.02	0.71	0.58	0.00	0.25	0.19	
	$\{OH^-,OH^-,HO_2^-:S_{23'}\}$	0	−0.04	0.58	−0.51	−0.02	0.01	−0.03	6.8
		1	0.17	0.55	0.50	0.06	0.22	0.29	
	$\{H_2O,OH^-,OH^-:S_{23},OH^-:S_{23'}\}$	0	0.57	0.00	−0.62	0.03	−0.08	0.08	−0.2
		1	0.61	−0.01	0.70	0.03	0.09	0.22	
PA	$\{OH^-,-,O_2^{2-}:C_3\}$	1/2	−0.50	0.33	0.41	−0.21	–	0.79	−5.1
		3/2	0.57	0.31	0.48	0.25	–	1.07	
	$\{OH^-,-,O_2^{2-}:C_{3'}\}$	1/2	−0.49	0.37	0.42	−0.20	–	0.85	−1.7
		3/2	0.57	0.47	0.37	0.25	–	1.07	

	Species	J							
	{OH⁻,H₂O,O₂²⁻:C₃}	1/2	−0.53	0.34	0.59	−0.18	0.07	0.69	−7.1
		3/2	0.56	0.32	0.65	0.20	0.09	0.83	
	{OH⁻,OH⁻,HO₂⁻:S₂₃'}	1/2	0.54	0.69	-0.55	0.24	0.03	-0.03	16.5
		3/2	0.56	0.81	0.65	0.26	0.17	0.18	
	{OH⁻,OH⁻,HO₂⁻:C⊥}	1/2	0.56	0.61	−0.54	0.21	0.00	0.03	−2.7
		3/2	0.57	0.65	0.59	0.22	0.21	0.32	
NI'	{−,−,O₂²⁻:C₃'}	1/2	0.04	0.10	0.17	–	–	0.63	–
	{H₂O,−,O₂²⁻:C₃'}	1/2	0.07	0.07	0.12	0.00	–	0.69	–
	{OH⁻,−,O₂²⁻:C₃'}	1/2	0.44	0.01	0.02	0.07	–	0.34	–
	{−,−,HO₂⁻:C₃'}	1/2	0.02	0.41	0.17	–	–	0.31	–
	{−,−,HO₂⁻:C₃'} H_up	1/2	0.00	0.03	0.53	–	–	0.30	–
	{H₂O,−,HO₂⁻:C₃'}	1/2	0.06	0.41	0.13	0.00	–	0.31	–
	{H₂O,−,HO₂⁻:C₃'} H_up	1/2	0.00	0.07	0.48	0.00	–	0.33	–
	{OH⁻,−,HO₂⁻:C₃'}	1/2	0.57	0.04	0.00	0.16	–	0.09	–
	{OH⁻,−,HO₂⁻:C₃'} H_up	1/2	0.02	0.09	0.40	0.01	–	0.39	–
	{H₂O,OH⁻,HO₂⁻:S₂₃'}	1/2	0.03	0.09	0.46	0.00	0.13	0.15	–
NI	{−,OH⁻,OH⁻:S₂₃,OH⁻:S₂₃}	1/2	0.65	−0.54	0.61	–	−0.03	0.29	3.2
		3/2	0.66	0.70	0.70		0.19	0.43	
	{H₂O,OH⁻,OH⁻:S₂₃,OH⁻:S₂₃}	1/2	0.65	−0.55	0.62	0.00	−0.02	0.26	3.0
		3/2	0.65	0.71	0.71	0.00	0.16	0.41	
	{OH⁻,OH⁻,OH⁻:S₂₃,OH⁻:S₂₃}	1/2	0.63	−0.58	0.57	0.16	−0.01	0.09	6.3
		3/2	0.64	0.64	0.64	0.17	0.23	0.32	
	{H₂O,−,O²⁻:C}	1/2	0.61	0.65	−0.70	0.01	–	0.34	9.2
		3/2	0.60	0.71	0.75	0.01		0.50	
	{OH⁻, −,O²⁻:C}	1/2	−0.39	0.54	0.54	−0.13	–	0.34	−22.6
		3/2	0.59	0.72	0.63	0.18		0.51	
	{OH⁻,H₂O,O²⁻:C}	1/2	−0.44	0.59	0.53	−0.12	0.00	0.30	−7.3
		3/2	0.60	0.66	0.58	0.16	0.05	0.50	
	{H₂O,H₂O,O²⁻:C}	1/2	0.52	0.63	−0.58	0.00	0.00	0.26	9.8
		3/2	0.59	0.70	0.65	0.00	0.09	0.54	
	{−,OH⁻,O²⁻:C}	1/2	0.37	−0.52	0.55	–	0.08	0.45	2.5
		3/2	0.38	0.58	0.66		0.32	0.73	
	{H₂O,OH⁻,O²⁻:C}	1/2	0.47	−0.53	0.55	0.00	0.03	0.35	9.9
		3/2	0.49	0.57	0.66	0.00	0.29	0.65	
	{OH⁻,OH⁻,O²⁻:C}	1/2	−0.55	0.54	0.57	−0.11	0.26	0.26	6.6
		3/2	0.60	0.56	0.61	0.12	0.25	0.52	
	{−,O²⁻,O²⁻:C}	1/2	0.02	−0.41	0.54	–	0.45	0.38	18.9
		3/2	0.08	0.55	0.61	–	0.97	0.61	
	{OH⁻,O²⁻,O²⁻:C}	1/2	−0.56	0.44	0.51	−0.10	0.54	0.17	3.1
		3/2	0.60	0.45	0.51	0.10	0.55	0.47	

Table 5. Calculated relative energies of the various complexes. Energies are given for structures optimized in vacuum (ΔE_{vac}), in a dielectric continuum (ΔE_{cosmo}), and with QM/MM methods. For the latter, energies are given for the isolated quantum system, studied in gas phase at the BP86/6-311+G(2d,2p) level (ΔE_{gas}), the change in the energy when the effect of the surrounding protein is included by an array of point charges ($\Delta\Delta E_{ptch}$), when the method is changed to B3LYP ($\Delta\Delta E_{B3lyp}$), and when the MM energy of system 2 is included ($\Delta\Delta E_{MM}$). Finally, two sets of total energies are given, with or without the $\Delta\Delta E_{MM}$ term. Thus, $\Delta E_{tot} = \Delta E_{gas} + \Delta\Delta E_{ptch} + \Delta\Delta E_{B3lyp}$, and $\Delta E_{totMM} = \Delta E_{tot} + \Delta\Delta E_{MM}$.

Ox state	Protonation state	Relative Energies (kJ/mol)							
		ΔE_{gas}	$\Delta\Delta E_{ptch}$	$\Delta\Delta E_{B3lyp}$	$\Delta\Delta E_{MM}$	ΔE_{tot}	ΔE_{totMM}	ΔE_{vac}	ΔE_{cosmo}
Ox	{H$_2$O,OH$^-$}	0	0	0	0	0	**0**	0	0
	{OH$^-$,H$_2$O}	33.5	51.0	−32.2	−12.1	52.2	**40.2**		
Ox	{OH$^-$,OH$^-$}	65.5	15.3	−14.4	−0.9	66.3	**65.5**	21.9[a]	51.1
	{H$_2$O,O^{2-}}	0	0	0	0	0	**0**	0	0
	{OH$^-$,OH$^-$:S$_{23}$}	−5.4	97.4	47.4	21.3	139.4	**160.7**		
	{−,OH$^-$:S$_{23}$,OH$^-$:S$_{23'}$}	−3.1	171.9	−19.8	13.6	188.5	**202.2**		
Red	{H$_2$O,−}	0	0	0	0	0	**0**		
	{−,H$_2$O}	−11.0	106.8	8.1	−44.9	103.9	**59.0**		
Red	{H$_2$O,OH$^-$}	0	0	0	0	0	**0**	0	0
	{OH$^-$,H$_2$O}	−11.0	106.8	8.1	−44.9	103.9	**59.0**	29.9[a]	37.7
	{−,H$_2$O,OH$^-$:S$_{23}$}	−5.9	305.6	18.2	60.1	317.9	**224.1**		
Red	{H$_2$O,H$_2$O}	0	0	0	0	0	**0**		
	{−,H$_2$O,H$_2$O:S$_{23}$}	5.1	198.8	10.1	−48.9	214.0	**165.1**		
PI	{H$_2$O,−,O$_2^{2-}$:C$_3$}	0	0	0	0	0	**0**	0	0
	{H$_2$O,−,O$_2^{2-}$:C$_{3'}$}	−4.3	12.5	0.5	−4.5	8.7	**4.2**	0	0
	{OH$^-$,−,HO$_2^-$:C$_3$}	49.7	79.1	−30.8	−40.5	98.0	**57.5**	72.1	25.9
	{OH$^-$,−,HO$_2^-$:S$_{23'}$}							39.5	64.5
	{H$_2$O,−,O$_2^{2-}$:S$_{23'}$}							diss.	57.1
PI	{H$_2$O,OH$^-$,O$_2^{2-}$:S$_{23}$}	2.4	92.0	2.2	−52.4	96.7	**44.2**		

	{H_2O,OH^-,O_2^{2-}:$S_{23'}$}	21.7	38.3	0.0	0.8	60.0	**60.8**		
	{H_2O,OH^-:A_3,O_2^{2-}:$C_{3'}$}	0	0	0	0	0	**0**	0	0
	{OH^-,OH^-,HO_2^-:$C_\perp$}	66.5	−12.7	11.5	56.8	65.3	**122.0**	10.1	2.2
PI	{H_2O,−,HO_2^-:C_3}	0	0	0	0	0	**0**		
	{H_2O,−,HO_2^-:C_3} H_up	86.8	−22.4	−42.5	5.0	22.0	**26.9**		
PI	{H_2O,OH^-,HO_2^-:S_{23}}	138.2	−79.1	14.9	55.5	74.0	**129.5**		
	{H_2O,OH^-,HO_2^-:$S_{23'}$}	154.6	−119.2	−10.9	62.0	24.4	**86.4**		
	{H_2O,H_2O:A_3,O_2^{2-}:$C_{3'}$}	0	0	0	0	0	**0**		
PI	{OH^-,−,O_2^{2-}:C_3}							0	0
	{OH^-,−,O_2^{2-}:$S_{23'}$}							38.0	52.9
PA	{OH^-,−,O_2^{2-}:C_3}	4.3	5.2	−0.9	3.0	8.6	**11.6**		
	{OH^-,−,O_2^{2-}:$C_{3'}$}	0	0	0	0	0	**0**		
PA	{OH^-,H_2O:A_3,O_2^{2-}:C_3}	0	0	0	0	0	**0**		
	{OH^-,OH^-,HO_2^-:$S_{23'}$}	131.2	70.9	-23.3	-30.1	178.8	**148.7**		
	{OH^-,OH^-,HO_2^-:$C_\perp$}	86.6	8.1	−41.6	−18.5	53.1	**34.7**		
NI'	{−,−,HO_2^-}	0	0	0	0	0	**0**		
	{−,−,HO_2^-} H_up	23.8	20.5	−12.2	20.0	32.2	**52.2**		
NI'	{H_2O,−,HO_2^-}	0	0	0	0	0	**0**		
	{H_2O,−,HO_2^-} H_up	11.9	14.2	−7.0	20.8	19.1	**39.9**		
NI'	{OH^-,−,HO_2^-}	0	0	0	0	0	**0**		
	{OH^-,−,HO_2^-} H_up	43.8	-10.0	39.1	18.2	72.8	**91.0**		
NI	{−,OH^-,O^{2-}:C}	44.3	9.2	−15.5	13.7	38.1	**51.7**		
	{OH^-,−,O^{2-}:C}	0	0	0	0	0	**0**		
NI'	{H_2O,H_2O:A_3,HO_2^{2-}:$C_{3'}$}	0	0	0	0	0	**0**		
	{H_2O,H_2O,HO_2^{2-}:$S_{23'}$}	17.9	6.0	15.1	53.5	39.0	**92.6**		
NI'	{H_2O,−,O_2^{2-}:$C_{3'}$}	0	0	0	0	0	**0**		
	{OH^-,−,HO_2^-:$C_{3'}$}	25.6	62.1	−22.2	−15.5	65.5	**50.0**		
NI	{H_2O,−,HO_2^-}	89.6	−93.9	27.8	2.6	23.4	**26.0**		
	{−,OH^-,OH^-:S_{23},OH^-:$S_{23'}$}	84.6	29.9	1.4	27.6	115.8	**143.4**	41.6	5.9
	{OH^-, H_2O,O^{2-}:C}	40.7	31.9	29.2	−14.4	101.8	**87.4**		
	{H_2O,OH^-,O^{2-}:C}	0	0	0	0	0	**0**	0	0

NI							
NI	{−,−,O_2H^-:$C_{3'}$}	0	0	0	0	0	**0**
	ts1	58.0	−3.0	23.0	4.0	78.0	**82.0**
	{−,OH^-,O^{2-}:C}	−56.4	−6.1	−5.5	30.0	−68.0	**−38.0**
NI	{OH^-,−,O_2H^-:$C_{3'}$}	0	0	0	0	0	**0**
	ts2	71.0	−4.0	30.0	−3.0	97.0	**94.0**
	{OH^-,OH^-,O^{2-}:C}	−96.2	−4.9	−16.5	13.9	−117.6	**−103.7**
NI	{−,−,O_2^{2-}:$C_{3'}$}	0	0	0	0	0	**0**
	ts3	84.0	32.0	8.5	−22.0	124.5	**102.5**
	{−,O^{2-},O^{2-}:C}	6.5	46.6	11.9	−14.9	65.0	**50.1**
NI	{OH^-,−,O_2^{2-}:$C_{3'}$}	0	0	0	0	0	**0**
	ts4	90.0	27.0	8.0	−22.0	125.0	**103.0**
	{OH^-,O^{2-},O^{2-}:C}	−33.3	61.0	−28.7	−30.2	−1.1	**−31.3**
NI	{H_2O,−,O_2H^-:$C_{3'}$}	0	0	0	0	0	**0**
	ts5	38.8	48.2	25.0	−24.0	112.0	**88.0**
	{H_2O,OH^-,O^{2-}:C}	−89.6	93.9	−27.8	−2.6	−23.4	**−26.0**

[a] Obtained with the three Cu–Cu distances fixed to 3.9 Å (Ox) or to the QM/MM (Red) values in Table 2.

TABLE OF CONTENTS GRAPHIC
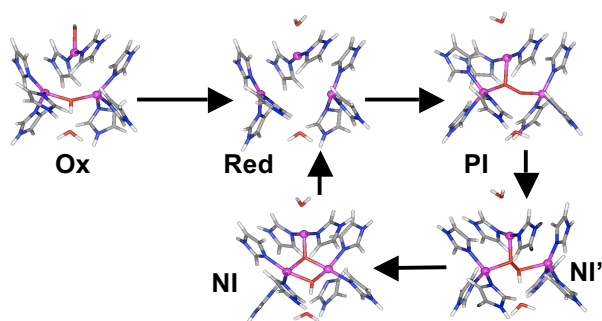
Structures of the various intermediates in the catalytic cycle of multi-copper oxidases (MCO) have been studied and characterized by QM/MM calculations. Together with the accompanying energetic data, it allowed us to propose a plausible reaction mechanism for the whole class of MCOs that is consistent with the experimental spectroscopic and structural data.